

Effects of microclimatic conditions and urban building configurations on aerodynamic characteristics and health risks of bioaerosols: Insights from idealized urban models

Zhijian Dong^a, Zhijian Liu^{a,*}, Chenxing Hu^b, Chenglin Ye^a, Yongjun Jin^a, Haiyang Liu^a, Rui Rong^a, Yuchen He^a, Li Chen^a, Chuanchen Li^a, Yaolong Shi^a, Yufeng Su^a

^a Department of Power Engineering, North China Electric Power University, Baoding, Hebei 071003, China

^b School of Mechanical and Vehicle Engineering, Beijing Institute of Technology, Beijing 100081, China



ARTICLE INFO

Keywords:

Wind tunnel test
Microclimatic factor
Building arrays
Bioaerosols
Quantitative microbial risk assessment

ABSTRACT

Urban biosafety faces substantial challenges, particularly regarding the aerodynamic behavior of bioaerosols influenced by microclimate and building layout, impacting human health, the environment, and climate. This study explores these effects through wind tunnel experiments and idealized urban models, focusing on bioaerosol aerodynamics. Concentrations are generally higher on the leeward side of buildings compared to street canyons. The incident wind direction affects the uniformity of bioaerosol distribution and migration trajectory within the building area. Increased wind speed from 1.36 to 2.54 m/s, the bioaerosol concentrations in different spatial locations decreased by 26.30 %-97.73 %. Quantitative microbial risk assessment, based on wind tunnel data, evaluates health risks across various age groups, revealing that adults consistently face higher risks than other groups. Increased wind speed from 1.36 to 2.54 m/s markedly reduces infection probability and disease burden by 1–2 orders of magnitude. Bioaerosol dispersion is influenced by wind direction, with a 45° angle improving bioaerosol uniformity and reducing health risks. Wind speed exerts a more significant impact on health risks than building layout or wind direction. This research offers a scientific basis for improving urban environment environmental quality and public health, supporting bioaerosol management, and the optimization of urban planning for enhanced biosecurity and sustainable development.

1. Introduction

With the acceleration of urbanization and population growth, urban biosafety related to bioaerosol transmission or biosafety activities has immeasurable impacts on human health, environment and climate (Ouyang et al., 2024, Yang et al., 2023, Zhou et al., 2019, Zhao et al., 2023, Teng et al., 2024). Notable incidents include the 1979 anthrax outbreak at the Sverdlovsk Biological Weapons Laboratory (Meselson et al., 1994), the 2003 SARS coronavirus outbreak at the laboratory breach in Singapore (Zumla et al., 2016), and the 2019 Brucella bioaerosol leakage at the Gansu Biological Pharmaceutical Factory (Xu et al., 2023), and other bioaerosol carrier leakage accidents. Additionally, terrorist activities have further complicated urban biosecurity (Luo & Qi, 2021, Tin et al., 2022). Consequently, investigating the aerodynamic characteristics of bioaerosols in urban environments is crucial for advancing biosafety measures and promoting sustainable urban

development.

The aerodynamic behavior of bioaerosols in urban environments is influenced by factors such as microclimate and building configuration (Smith et al., 2012, Liu et al., 2023a, Morawska et al., 2022, Lee & Mak, 2021, Keshavarzian et al., 2021). Lee and Mak (Lee & Mak, 2021) examined how wind direction and building array configuration affect airflow and pollutant dispersion in the central spaces of L-shaped and U-shaped structures, concluding that L-shaped arrays more effectively dilute pollutants compared to U-shaped arrays. Keshavarzian et al. (Keshavarzian et al., 2021) explored the impact of building cross-sectional shapes on pollutant diffusion around isolated buildings, finding that circular and curved structures have a smaller lee critical emission zone compared to chamfered and square buildings. Hang and Chen (Hang & Chen, 2022) assessed the urban microclimate within street canyons of varying aspect ratios, discovering that increased aspect ratios decrease convective airflow and increase radiative flux. Zhong

* Corresponding author.

E-mail address: zhijianliu@ncepu.edu.cn (Z. Liu).

et al. (Zhong et al., 2023) analyzed how semi-open street roofs in two-dimensional canyons affect CO gas exposure and pedestrian thermal comfort. Xiao et al. (Xiao et al., 2024) investigated the dynamic effects of tree shape and canyon geometry on pedestrian thermal comfort. Chen et al. (Chen et al., 2023) compared the impacts of uniform versus non-uniform surface heating on airflow and ventilation in canyons through numerical simulations and scaled outdoor experiments, highlighting that thermal buoyancy significantly influences airflow patterns. Xu et al. (Xu et al., 2024) assessed the impact of urban form on the thermal environment of Hong Kong communities, noting that daytime thermal conditions are predominantly influenced by two-dimensional parameters (e.g., impervious surface area), while nighttime conditions are affected by both two-dimensional and three-dimensional parameters (e.g., sky view factor and road density). Previous research has predominantly focused on how microclimate affects airflow and gaseous pollutants dispersion around isolated structures and street valleys, pedestrian thermal comfort and thermal environments, with a heavy reliance on numerical simulations.

Although some studies have evaluated bioaerosol transmission risks in urban areas (Zhang et al., 2021), they often use aggregated meteorological conditions, making it challenging to interpret the influence mechanism of a single variable. Studies have shown that building layout can significantly influence local airflow and ventilation patterns in urban environments, thereby impacting bioaerosol dispersion (Bouketta & Bouchahm, 2020). Zhang et al. (Zhang et al., 2020a) further elucidated that changing the building layout can enhance bioaerosol dispersion while reducing exposure risks for nearby individuals. Gao et al. (Gao et al., 2024) examined the dispersion characteristic of bioaerosols around landfill sites, revealing that microclimatic conditions impact their spread to adjacent areas. Furthermore, Liang et al. (Liang et al., 2023) demonstrated that fluctuations in microclimate affect both the dispersion and viability of bioaerosols. Fraczek et al. (Fraczek et al., 2014) confirmed that microclimatic factors play a critical role in determining the pathogenicity of airborne bioaerosols. Thus, the impacts of specific factors like microclimate and building layout on bioaerosol aerodynamics and associated health risks require further investigation. Additionally, there is a notable absence of experimental data to substantiate existing theoretical models.

There are three main methods to study urban pollutant dispersion: field measurement (Zhang et al., 2024), wind tunnel experiments (Zhao et al., 2024a, Zhang et al., 2020b) and computational fluid dynamics (CFD) simulations (Dong et al., 2024, Huertas et al., 2021, Zheng et al., 2021). Field measurements, while straightforward, are costly and can be significantly affected by complex natural phenomena (Lee & Mak, 2019). CFD simulations, though valuable, depend heavily on the accuracy of the simulated environment and model selection (Tominaga & Stathopoulos, 2013) and require empirical data for validation. The advent of machine learning holds promise for predicting bioaerosol behavior in urban settings (Lin et al., 2024), but this approach also depends on the availability of training datasets. For the particulate dispersion test, although some researchers consider the use of tracer gases to simulate the diffusion behavior of solid particles with diameters smaller than 1×10^{-6} m in urban environments as a viable approach (Nielsen, 2009), the applicability of this method is still questioned. Bioaerosol aerodynamics is the key to cutting the transmission chain of biosecurity risks (Xie et al., 2020). At present, the aerodynamic migration mechanism of bioaerosols in urban environments is still lacking experimental verification (Zhao et al., 2024a). Although the cost of wind tunnel experiments is relatively high, the experimental conditions are controllable, and the data are reliable (Blocken et al., 2016, Zhao et al., 2022). Wind tunnel experiments have been extensively employed in the wind field and structural research of low-rise and high-rise buildings, and the experimental results are often used to verify the reliability of numerical simulations of wind fields in complex terrain (Khattak et al., 2023, Bezabeh et al., 2018). Therefore, employing scaled models of idealized urban wind tunnels for bioaerosol dispersion experiments is a

feasible method to fill this gap.

This study proposes a wind tunnel experiment method using scaled-down models to simulate the dispersion behavior of bioaerosols in an ideal urban model. The aim is to address the following research gaps: Firstly, providing high-fidelity data for flow field reconstruction and providing an experimental basis for numerical model verification and machine learning training. Secondly, elucidating the specific impacts of microclimate and building layout on the aerodynamic migration characteristics of bioaerosols. Thirdly, assessing health risks across different age groups using quantitative microbiological risk assessment methods. Lastly, exploring the sensitivity of microclimate and building layout to health risks. This study contributes to a deeper understanding of the aerodynamic characteristics of bioaerosols in urban environments under the influence of microclimate and building layout. They facilitate accurate prevention and control of urban biosafety issues, safeguarding urban residents' health and promoting sustainable urban development.

2. Materials and methods

The overall research framework is outlined as follows: First, the bioaerosol required for the wind tunnel experiments is prepared. Then, the wind tunnel experiments are conducted, comprising: 1) high-fidelity flow field experiments; 2) a pre-experiment to validate the accuracy and effectiveness of the bioaerosol dispersion experiment; 3) an investigation into the aerodynamic migration patterns of bioaerosols under single-variable conditions such as microclimate and building layout. Finally, the results are analyzed to propose recommendations for sustainable urban development. The detailed research framework is illustrated in Supplementary Materials Fig. 1.

2.1. Wind-tunnel modeling

Wind-tunnel experiments are performed for the ideal city model in the atmospheric boundary layer wind tunnel at North China Electric Power University, see Fig. 1. The wind tunnel comprises distinct sections: intake, high-speed test, power, stable, contraction, low-speed test, and tail diffusion (Fig. 1(a)). Operating conditions allow for theoretical maximum wind speeds of 30 m/s in the high-speed test section and 20 m/s in the low-speed test section. Due to its larger cross-sectional area, the study focused on the low-speed test section, which spans approximately 10.7 m in length with dimensions of 1.48 m width and 1.4 m height (Fig. 1(b)). The spires and rough elements upstream of the test section shown in Fig. 1(c) are used to generate atmospheric boundary layer flow and turbulence (Bendjebbas et al., 2016). Fig. 1(d) illustrates that air velocity varies inversely with temperature and directly with relative humidity. Studies indicate that the average air speed in urban environments ranges from 0.5 to 3.5 m/s (Qiao et al., 2023, Maing, 2022). Baş et al. (Baş et al., 2024) have highlighted that higher wind speeds enhance outdoor ventilation, while lower speeds contribute to pedestrian wind comfort. Considering the pedestrian wind comfort and bioaerosol dispersion, this study utilizes air velocities of 1, 2, and 3 m/s to examine the impact of microclimate on the aerodynamic characteristics of bioaerosols. This analysis aims to provide a scientific foundation for effective urban biosafety measures and to support sustainable urban development. At the specified air velocities, the measured vertical airflow in the building vicinity reaches approximately 0 to 3.5 m/s. The reference wind speeds at building height $H = 0.125$ m are $U_{ref1} = 1.36$ m/s, $U_{ref2} = 2.09$ m/s and $U_{ref3} = 2.54$ m/s, respectively. As depicted in Fig. 1(e), higher reference wind speeds correspond to lower relative wind speeds (MU). Moreover, within the vertical region, relative wind speed shows an inverse proportionality to turbulence intensity.

To ensure the validity and reliability of the experimental results, the wind tunnel experiment must adhere to geometric, kinematic, and dynamic similarity principles for the building model (Zhao et al., 2022, Cui et al., 2021). In this study, the architectural model is scaled at 1:200 (Fig. 2), meeting the geometric similarity criterion. The upstream wind

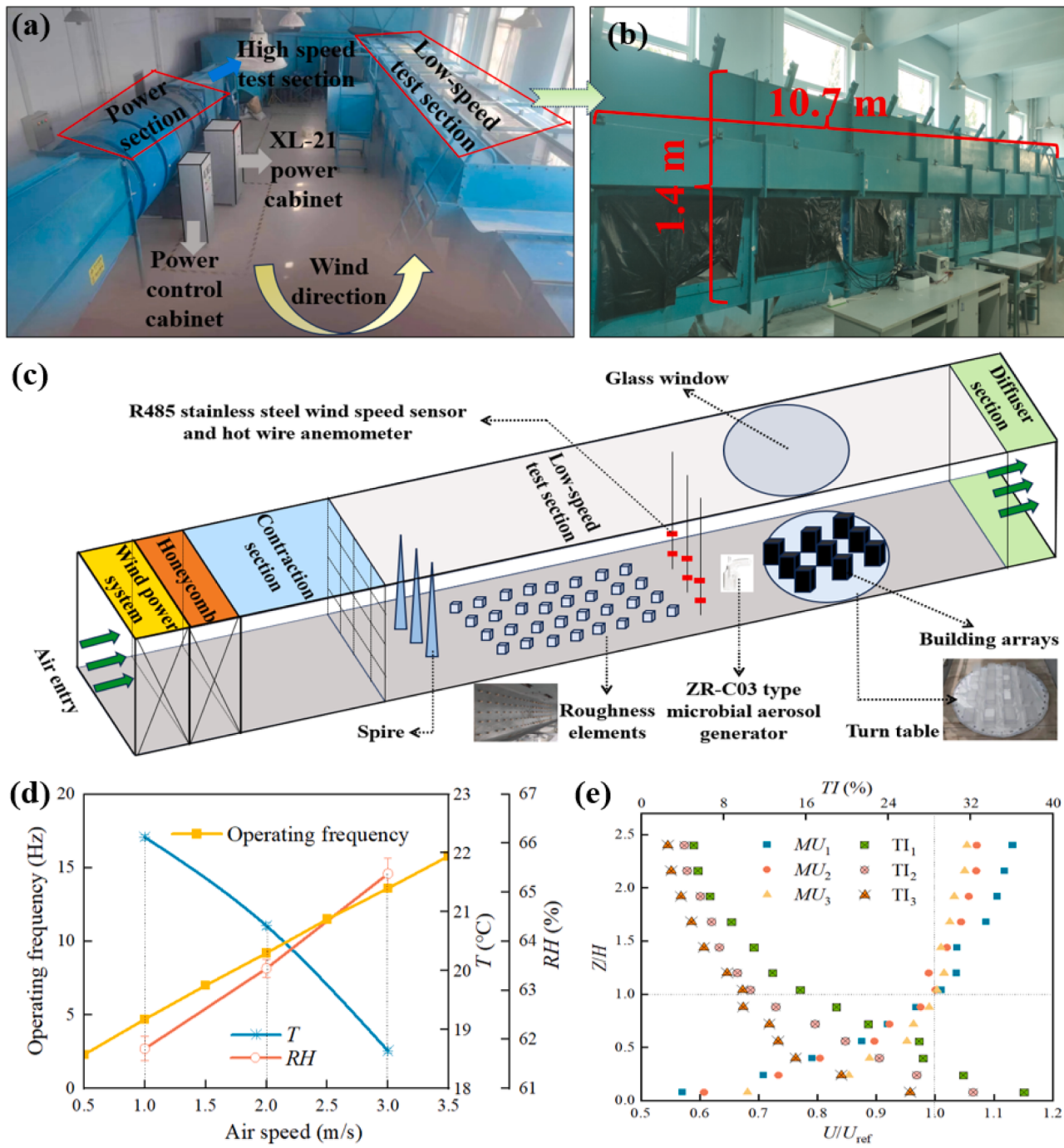


Fig. 1. Boundary layer wind tunnel and characteristic parameters. (a) Top view of the wind tunnel; (b) Low-speed test section; (c) Schematic diagram of the interior of the test section; (d) Boundary layer meteorological parameters; and (e) dimensionless mean streamwise velocity and turbulence intensity distribution of incident vertical profiles.

velocity profile and turbulence intensity within the test section, shown in Fig. 1(d), align with the required motion similarity characteristics. For three reference wind speeds, the corresponding Reynolds numbers for building height are $Re_{H1} = 11\,553$, $Re_{H2} = 17\,702$ and $Re_{H3} = 21\,496$, all of which are higher than the critical Reynolds number $Re_c = 11\,000$ (Zhao et al., 2022), thus satisfying dynamic similarity conditions. The higher the reference speed, the stronger the Re independence of the flow. Additionally, the maximum blockage ratio for the building layouts ($\varphi_{max} = A_{max}/A_t$ = the maximum upwind area/cross-sectional area of the wind tunnel section of the test model) is 2.41 %, which is below the 5 % threshold (Cui et al., 2021), indicating that the blockage effect is

negligible.

In the low-speed test section, three building configurations— 3×3 , 4×4 , and 3×5 —were constructed for experimentation. Fig. 2 depicts the schematic diagram of the ideal urban model, along with its experimental monitoring and spatial sampling points. To investigate the influence of varying wind directions on pollutant spatial distribution, the study manipulated wind direction by rotating the turntable during experiments, introducing incident angles of 0° , 45° , and 90° , respectively.

Meteorological parameters such as wind speed, temperature, and relative humidity at the inlet of the test section are measured by the following instruments, whose performance parameters are shown in

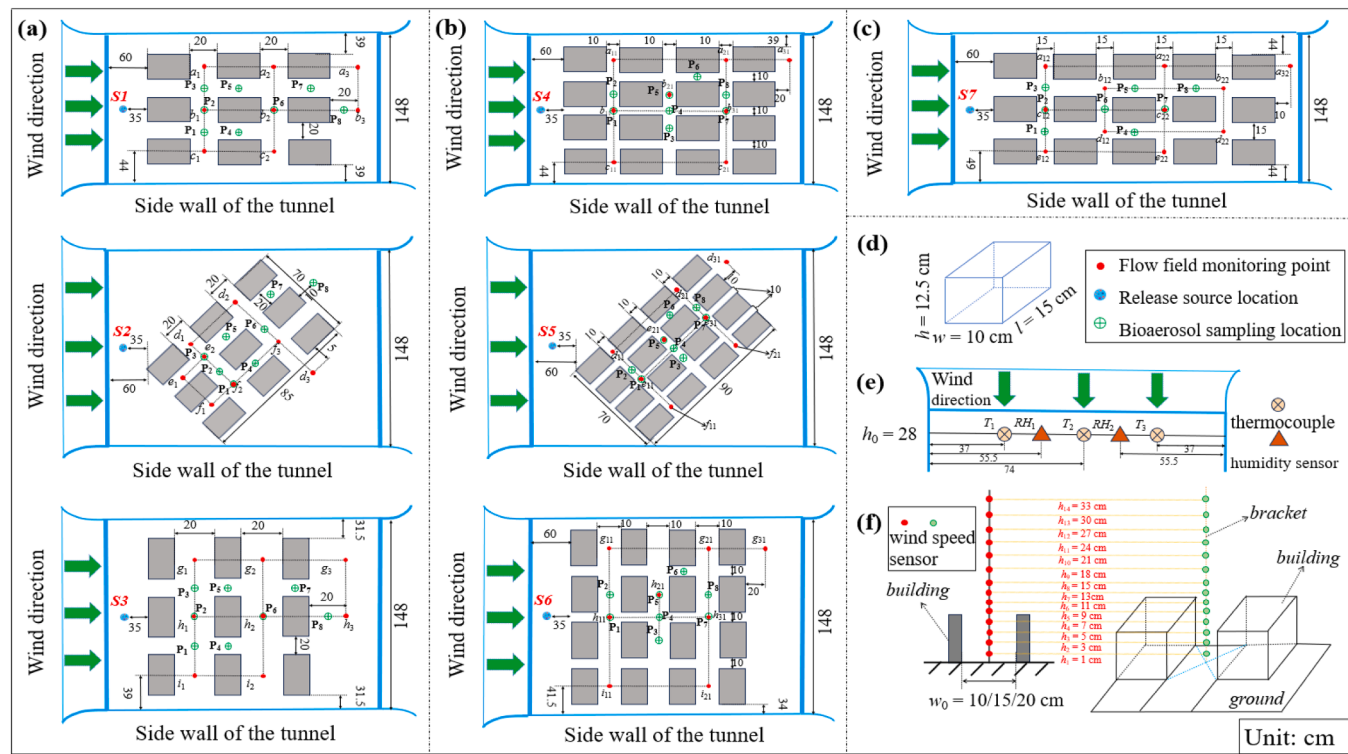


Fig. 2. Schematic diagram of the ideal urban model, along with its experimental monitoring and spatial sampling points. (a) 3 × 3 building array; (b) 4 × 4 building array; (c) 3 × 5 building array; (d) The basic characteristic unit of the building group; (e) meteorological parameter monitoring point and (f) airflow monitoring point. The building arrays of 3 × 3 and 4 × 4 configurations are each exposed to three incident wind directions: 0°, 45°, and 90°, denoted as 3 × 3-0°, 3 × 3-45°, 3 × 3-90° and 4 × 4-0°, 4 × 4-45°, 4 × 4-90°, respectively.

Table 1

The performance parameters of instruments.

Experiment	Instrument	Types	Range	Accuracy	Physical drawing
Flow field measurement phase	Stainless steel wind speed sensor	RS485	0–30 m/s	±3 %	
	Temperature sensor	WZP-Pt100	-50–200 °C	±0.15 + 0.002 T	
	Humidity sensor	Z2000	5 %–95 % RH	±5 % RH	
	Data acquisition device + direct connection unit	LR8450 + U8551	1–120 ch	1 ms	
	Linear DC power supply	UTP3305-II	0–30 V; 0–5 A	<0.01 %+3 mV; ≤0.2 %+3 mA	

Table 1. During the experiment, the XL-21 power cabinet (see Fig. 1(a)) was utilized to control the operating frequency of the wind tunnel, enabling precise regulation of wind speeds ranging from 0.5 to 3.5 m/s based on the established relationship between frequency and wind speed. During the measurement phase, the wind tunnel was meticulously sealed to ensure the accuracy of the experimental results. The indoor temperature and humidity were maintained as constant as

possible, and the orientation of the wind was aligned with that of the high-precision wind speed probe to enhance measurement accuracy. Initially, the model and wind speed probe were positioned within the wind tunnel. The wind tunnel was then activated to stabilize the flow field, minimizing errors from fluctuations in incoming flow velocity and ensuring ambient conditions remained stable. The wind speed probe was affixed to an acrylic plate at a fixed height (refer to Fig. 2(f)) to prevent

discrepancies related to probe height adjustments. Following a stabilization period of 10 minutes, measurements commenced for 5 minutes, during which a total of 300 data points were collected at each measurement location. Outliers within the dataset were systematically identified and addressed to maintain data integrity, after which the average wind speed was computed for each measurement point. Through a series of repeated operations, the wind speed profiles along the vertical axis of each spatial position were obtained across different configurations. Additionally, three temperature sensors and two humidity sensors (see Fig. 2(e)) were strategically placed at equal intervals 60 cm from the model at the wind tunnel entrance to record average temperature and humidity throughout the experimental section. During the experiment, a release source was consistently positioned 35 cm from the building front, with eight spatial sampling points within the building area designated for bioaerosol collection. Supplementary Materials Table 1 presents the location coordinates of these bioaerosol sampling points across different experimental scenarios.

2.2. Bioaerosol generation, release, collection and cultivation

Serratia marcescens is a bioaerosol particle with actual biological attributes, and its particle size distribution also meets the characteristics of bioaerosol. At the same time, the colony of this strain after culture was red and could be easily distinguished from other miscellaneous bacteria (Liu et al., 2023b; de Ondarza, 2017). Therefore, *Serratia marcescens* was chosen as a bioaerosol tracer from the Academy of Military Sciences as a bioaerosol tracer in this study. The specific links of the bioaerosol dispersion experiment are shown in Fig. 3. To prevent potential contamination from airborne microorganisms during experiments, the high-speed and low-speed test sections of the wind tunnel were thoroughly sterilized using ultraviolet germicidal lamps. Each has a 30-minute killing time before and after each trial (Elimination time is confirmed in Supplementary Materials Table 2) to eliminate any potential effects of residual bacteria that may have been introduced during the initial phase. Precisely, after the end of the experiment, three ultraviolet lamps were positioned downstream of the low-speed test section, and the two ultraviolet kill lights of the high-speed test section were made sure to be on, all operating for an additional 30 minutes. Throughout the wind tunnel operation, all five lamps remained activated to ensure continuous sterility. Furthermore, to ensure the reliability and reproducibility of results, three parallel experiments were conducted in each group, resulting in a total of 63 experimental groups.

Bioaerosol generation: a) Bioaerosol recovery preparation: Take a

little bacterial liquid from the frozen tube and put it into a test tube (built-in 10 mL nutrient broth), and put the test tube into an oscillating incubator (37°C , 200 rpm) for 18 h b) Titer experiment: *Serratia marcescens* solution was reversely diluted with PBS buffer. Following dilution, 1mL of the mixture was absorbed and poured into a solid culture dish (13.2 g nutrient AGAR / 400 mL distilled water). The solid culture dish was covered with a layer of semi-solid culture solution (2.4 g AGAR powder / 400 mL distilled water + 7.6 g nutrient broth / 400 mL distilled water). After solidification, the petri dish was turned upside down and cultured in a biochemical incubator (37°C) for 18–24 h c) Glycerol cryopreservation was employed post-counting. e) Prior to the diffusion experiment, the known concentration of the bacterial solution was further diluted using an eyedropper, resulting in a 50 mL bacterial solution (concentration 10^5 CFU/mL) prepared for use.

Bioaerosol release: The bioaerosol solution is transferred into a microbial aerosol generator (type ZR-C03) powered by an aerosol generator (ZR-1050). The performance parameters of relevant instruments are detailed in Table 2. The bioaerosol release was conducted at a position 0.35 m anterior to the model (refer to Fig. 2), with the generator outlet positioned at a height of 0.09 m and a release velocity set to 1 m/s. The duration of bioaerosol release for the experiment was 5 min. To mitigate potential interference from recirculated bioaerosols on subsequent sampling accuracy, two ultraviolet kill lamps (TDZ-201), maintained in continuous operation, were strategically positioned within the high-speed test section of the wind tunnel during the bioaerosol release phase.

Bioaerosol collection and culture: Eight sampling locations were designated within each building array (Fig. 2) for culturable *Serratia marcescens* measurements. When the release time is 5 min, simultaneous sampling was conducted at these 8 points. Bioaerosols were collected using an intelligent microbial sampler (ZR-2002) and an air microbial absorption bottle with 8 mL PBS buffer (AGI, ZR-B02) (Table 2). Sampling was performed at a height of 0.08 m with a flow rate of 7 L/min for 2 min. The above steps were repeated after each group of experiments, and three groups of parallel experiments were carried out.

Given the spatial constraints within the wind tunnel and the dimensions of the sampling equipment, direct placement of the sampling apparatus in the experimental section could disrupt the flow field. To alleviate this problem, we positioned the air microbial absorption bottle at the model's tail and utilized a clean plastic hose, 1.2 m in length and 0.01 m in diameter, at the sampling port. This configuration effectively mitigates the impact of larger volumes on flow dynamics. To enhance

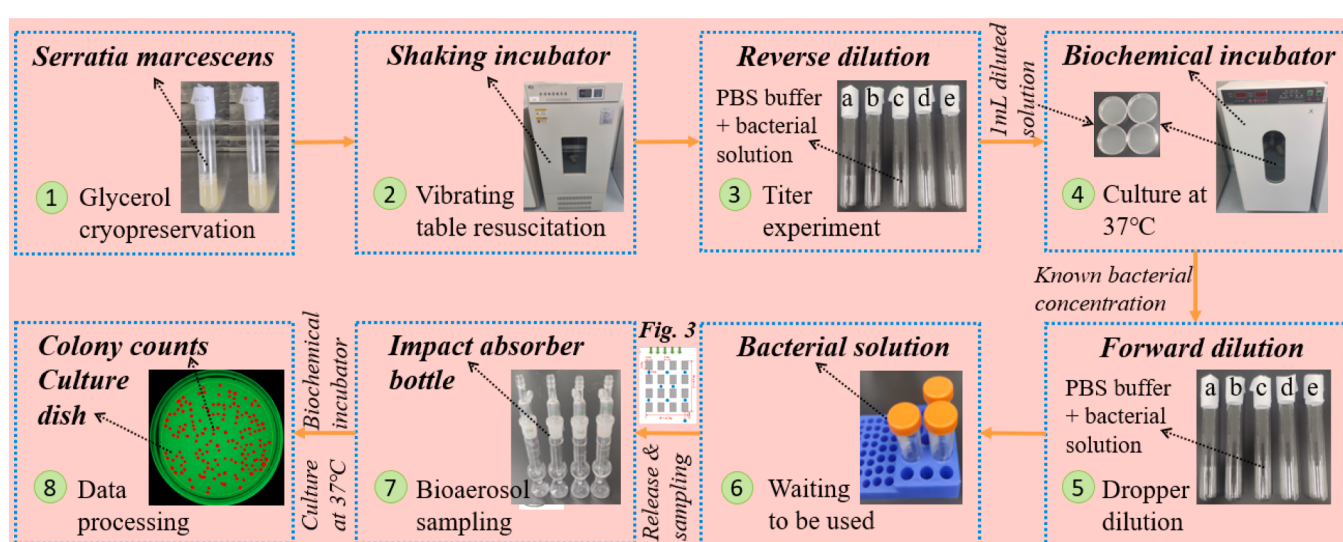


Fig. 3. The specific link of the bioaerosol dispersion experiment.

Table 2

The performance parameters of the instruments.

Experiment	Instrument	Types	Range	Accuracy	Physical drawing
Bioaerosol release phase	Aerosol generator	ZR-1050	8–12 L/min	±2.5 %	
	Aerosol dispenser	ZR-C03	8–12 L/min	±0.05 m/s	
	Laser dust particle counters	PGM-300	0–999 ug/m³	≤ ±1 %	
Bioaerosol sampling phase	UV light sterilizer	TDZ-201	50–60 Hz		
	Intelligent air microbial sampler	ZR-2002	0–50 L/min	±2.5 %	
	Air Microbial Absorption Bottle (AGI)	ZR-B02	7 L/min		

data collection accuracy and account for varying meteorological conditions, we introduced a sampling correction factor λ (λ = sampling quantity from air microbial absorption bottle/sampling quantity from 1.2 m clean plastic hose). Using the 4 × 4 building arrays as a case study, a total of 36 experimental trials were conducted to establish the sampling correction coefficient under varying wind speeds and directions while also considering the effects of temperature and humidity. Detailed findings are presented in Supplementary Materials Figs. 2 and 3. The results indicate that wind speed is the primary factor influencing the sampling correction coefficient. Since the exact specification of a clean plastic hose was employed for sampling across all spatial positions, variations in other meteorological parameters did not significantly affect the coefficient. Consequently, for the three tested wind speeds, the sampling correction coefficients were determined to be 2.9, 2.4, and 2.0, respectively.

After sampling, 1mL of bacterial liquid from the air microbial absorption bottle was loaded into the petri dish containing malt extract agar with 1mL pipette, and the heated semi-solid medium ((2.4 g agar powder + 7.6 g nutrient broth) / 400 mL distilled water) was poured on it and shaken well. After solidification, the petri dish was turned upside down. Incubate in a constant temperature (37 °C) incubator for 18–24 h. Colony forming units (CFU) from each petri dish were enumerated and expressed as CFU per cubic meter of air (CFU/m³). The concentration of bioaerosols in the air is calculated as follows:

$$C_{\text{average}} = (\lambda_i \times N \times 1000) / (T \times F) \quad (1)$$

where C_{average} represents the average bioaerosol concentration from the three parallel experiments at each sampling location (CFU/m³), N denotes the number of colonies on the petri dish corresponding to each sampling location (CFU), T is the sampling time (min), and F is the sampling flow rate (L/min). λ_i represents the ratio of the sampling quantity of air microbial absorption bottle to that of 1.2m clean plastic hose under different wind speeds. Here, $i = 1, 2$ and 3 corresponds to wind speeds of 1, 2, and 3 m/s, respectively. Specifically, λ_1, λ_2 and λ_3 are 2.9, 2.4 and 2.0, respectively (refer to Supplementary Materials Figs. 2 and 3).

To visually analyze the spatial distribution of bioaerosols across different building arrays, the concentration of bioaerosol is represented by the dimensionless value K_c , whose expression is as follows:

$$K_c = C_{\text{average}} / C_{\text{source}} \quad (2)$$

where K_c represents the dimensionless concentration, and C_{source} is the bioaerosol concentrations of the release source (CFU/m³). The source concentration was approximately 4.85×10^5 CFU/mL.

2.3. Quantitative microbial risk assessment

Combining bioaerosol distribution characteristics to quantify the risk of microbial transmission is crucial for urban environmental biosafety prevention and control. The quantitative microbial risk assessment (QMRA) model has been widely applied to evaluate infection risk among human populations within built environments (Liu et al., 2023c). While numerous studies have focused on indoor or semi-open settings such as subways (Miller et al., 2022), office buildings (Salunkhe et al., 2024), hospitals (Perez et al., 2015) and residences (Ali et al., 2022a), there remains a relative scarcity of research addressing microbial exposure risks in broader urban contexts.

Based on this, the QMRA model was applied in this study to evaluate the infection risk and disease burden across various age groups exposed to differing building layouts, specifically in the context of microclimatic influences. The QMRA framework encompasses four key steps: hazard identification, exposure assessment (dose of pathogen exposure), dose-response assessment (the annual probability of infection $P_{(y)}$ and disease burden (DB)), and risk characterization (two benchmarks: the U.S. Environmental Protection Agency (EPA) ($P_{(y)} \leq 10^{-4}$ ppy), the WHO ($DB \leq 10^{-6}$ disability-adjusted life year [DALY] ppy) (Ali et al., 2022a, Gonzales-Gustavson et al., 2019, Yan et al., 2024)). The calculation parameters of quantitative microbial risk assessment are shown in Tables 3 and 4. The pathogenic microorganisms concerned in this study are derived from bioaerosols accidentally leaked in urban environments. In urban environments, individuals of all ages exposed to diverse building layouts may encounter significant health risks due to microclimatic

Table 3

Breathing rate is based on various age groups (Ali et al., 2022b; Xu et al., 2021).

Parameters	Pre-kindergarten	Elementary	Secondary	Adult	Elder
Age (years)	3–5	5–11	11–18	20–30	≥60
Breathing rate (m ³ /h)	0.303	0.416	0.595	0.777	0.569

influences. *Serratia marcescens*, a Gram-negative bacterium, is used as a tracer due to its potential to cause lung infections, urinary tract infections, and septicemia (Guo et al., 2020). Given its similarities, the dose-response model for *Escherichia coli*, also a Gram-negative bacterium (Duan et al., 2023), was adapted to approximate the infection probability associated with *Serratia marcescens*. The average exposure dose of inhaled bacteria for individuals at different spatial locations in urban areas is calculated as follows (Ali et al., 2022a; Li & Tang, 2022):

$$d_i = C_{\text{average}} \times BR \times T_i \times AI \quad (3)$$

where d_i is the average exposure dose (CFU), C_{average} represents the average bioaerosol concentration from the three parallel experiments at each sampling location (CFU/m³), BR is the Breathing rate (m³/h), T_i is the exposure time at each sampling site per day (h), AI is the ingestion rate.

Currently, QMRA methods primarily incorporate two dose-response models for assessing the health risks of specific pathogens, namely the exponential dose-response model and the beta-Poisson model (Ryan et al., 2014). The beta-Poisson model is more suitable for evaluating the infection risk of Gram-negative bacilli, and the corresponding expression is as follows (Yan et al., 2024; Shi et al., 2018):

$$P_{i(d)} = 1 - \left[1 + \frac{d_i}{N_{50}} (2^{1/\alpha} - 1) \right]^{-\alpha} \quad (4)$$

where $P_{i(d)}$ represents the daily infection probability of each spatial location, α and N_{50} are the model parameters. N_{50} represents the average dose to cause an infection.

The Monte Carlo simulation is employed to develop a probability-based risk model for the quantitative assessment of annual infection risk and disease burden (Islam et al., 2021). All calculations were performed by using Crystal Ball and Microsoft Excel 2016 in this study (Devleesschauwer et al., 2014). Input parameters, including exposure concentration and respiratory rate, were randomly selected from their respective probability distributions (Pasalari et al., 2019). Output parameters, such as annual infection probability and disease burden, were computed over 10,000 iterations to ensure the distribution reached a stable state. Utilizing a dose-response model for risk characterization, the expression for infection probability per person per year is formulated as follows (Yan et al., 2024):

$$P_{(y)} = 1 - (1 - P_{i(d)})^f \quad (5)$$

where $P_{(y)}$ represents the probability of being infected after a yearly exposure (pppy), f represents the annual frequency of each exposure scenario per year.

The specific potential disease burden caused by exposure to bioaerosols in different building layouts is calculated by using Eq. (6) (Yan et al., 2024; Havelaar et al., 2015).

$$DB = P_{(y)} \times HB \quad (6)$$

where DB represents the disease burden (DALYs pppy), HB represents the health burden that is expressed in DALYs per illness case (DALYs/case).

3. Results and discussion

3.1. Airflow distribution between different building arrays

Previous studies have shown that incoming wind speed, wind direction and building layout have significant effects on airflow patterns around buildings (Abohela et al., 2013; Ledo et al., 2011). These airflow patterns and building configurations directly impact the dispersion and spatial distribution of bioaerosols (Liu et al., 2023a; Liu et al., 2023d; Zhao et al., 2024b). Thus, the airflow distribution between different building arrays was measured in this study under three directions and wind speeds through wind tunnel scaling experiments, as shown in Fig. 4. When the building layout, wind speed and wind direction are constant, with the increase of vertical height, the wind speed in the near-formation area with $Z/H \leq 1$ is relatively lower and the change is more drastic than that in the region with $Z/H > 1$. This disparity is primarily attributed to building obstruction and the aerodynamic effect of airflow encountering building fronts, leading to the formation of a wake region downstream that alters local airflow organization and turbulence characteristics (Peterka et al., 1985). This phenomenon is more pronounced in the lee-side areas of buildings than in the street valleys between buildings.

Under identical building layouts and wind directions, wind speeds between building arrays increase gradually with higher incoming wind speeds. It is noteworthy that the escalation of wind speed generally does not significantly alter the vertical distribution pattern of airflow. However, in the near-ground region where $Z/H \leq 1$, the ratio $U/U_{\text{ref}3}$ exceeds that of $U/U_{\text{ref}1}$ and $U/U_{\text{ref}2}$, while within the same near-ground region, $U/U_{\text{ref}3}$ exhibits a smaller magnitude. Under consistent building layout and wind direction, wind speeds between building arrays progressively increase with higher incoming wind speeds. Notably, the increase in wind speed generally has minimal impact on the vertical airflow distribution trend. However, in the near-ground region where $Z/H \leq 1$, the ratio $U/U_{\text{ref}3}$ surpasses that of $U/U_{\text{ref}1}$ and $U/U_{\text{ref}2}$, while in areas where $Z/H > 1$, $U/U_{\text{ref}3}$ exhibits a lesser magnitude. Under consistent building layout and wind speed conditions, wind directions at 0° and 90° angles exhibit minimal influence on the vertical airflow distribution trend along the lee side of the building array and within the street valley, as depicted in Fig. 4 (a), (c), (d), and (f). In contrast, at a 45° wind angle, airflow can ingress into the building array, creating complex eddies that extend to the lee side and thereby increasing local wind speeds (illustrated in Fig. 4 (b) and (e)). This result indicates that the inclined wind is conducive to facilitating airflow penetration and ensuring adequate ventilation within the building array. This finding is consistent with the research presented in the literature (Lee & Mak, 2021). Furthermore, changes in wind direction significantly impact local airflow characteristics (Xie et al., 2023).

Fig. 4 illustrates that when the wind speed and direction are constant, the airflow between the 3 × 3 and 3 × 5 building arrays is more robust compared to that between the 4 × 4 building arrays, particularly noticeable in the near-ground area where $Z/H \leq 1$. This disparity arises

Table 4

Parameters for quantitative microbiological risk assessment.

Parameters	Ingestion rate (AI)	Exposure time (T)	Model parameters (N50)	Model parameters (α)	Exposure frequency (f)	Health burden (HB)
Values Reference	0.5 % (Ali et al., 2022b)	5 min	8.6 × 107 (Irda Sari et al., 2018)	0.155 (Shi et al., 2018)	365 (Ali et al., 2022a; Yan et al., 2024)	0.0455 (Yan et al., 2024; Havelaar et al., 2015)

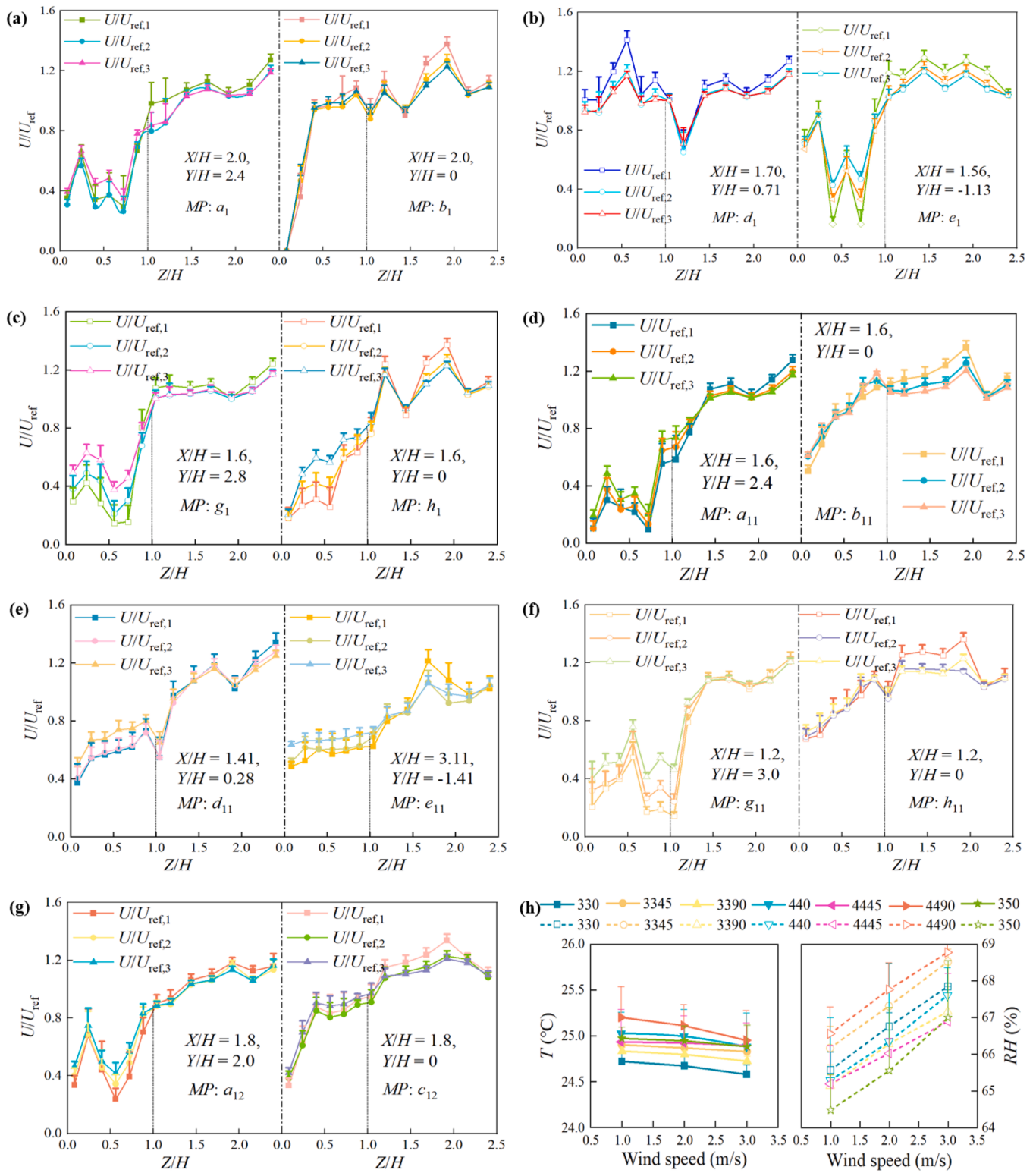


Fig. 4. Profiles of mean velocity between different building arrays under three directions and wind speeds. (a) $3 \times 3-0^\circ$; (b) $3 \times 3-45^\circ$; (c) $3 \times 3-90^\circ$; (d) $4 \times 4-0^\circ$; (e) $4 \times 4-45^\circ$; (f) $4 \times 4-90^\circ$; (g) $3 \times 5-0^\circ$; (h) $4 \times 4-0^\circ$. The symbol *MP* in Fig. 4 is the abbreviation of the monitoring point. In Fig. 4(h), the numbers 330, 3345 and 3390 represent the case of a 3×3 array with an inlet wind direction of 0° , 45° and 90° , respectively. For 4×4 and 3×5 arrays, numbers have the same meaning as for 3×3 arrays.

primarily from the narrower spacing between the 4×4 array, which intensifies the wind shadow effect behind the buildings. Overall, the airflow distribution pattern shows a significant correlation with wind speed, wind direction and building layout. The airflow distribution at other measured locations between different building arrays can be found

in Supplementary Materials Fig. 4. It can be seen from Fig. 4(h) that under the condition of the same building layout and inflow direction, the increase of wind speed will lead to a slight decrease in temperature. The possible reason is that when the wind speed increases, the diffusion ability of air flow will be enhanced, resulting in a reduction of

temperature (Zhang et al., 2022). In addition, the increase in wind speed leads to the rise of relative humidity due to the decrease in ambient temperature, which is consistent with the research conclusion of Fatemi et al. (Fatemi & Jebali, 2022). As depicted in Fig. 4(h), variations in temperature and humidity distributions are observed under different building layout conditions, which can be attributed to differences in time intervals between measurements. However, these differences are relatively minor and are assumed to have a negligible impact on the experimental results. The temperature and humidity parameters observed during the experiments for various building layouts are presented in Fig. 4(h), aiming to provide reliable data for scholars engaged in reconstructing high-fidelity flow fields.

3.2. Spatial distribution of bioaerosols

Fig. 5 presents the dimensionless concentration of bioaerosols measured at eight spatial locations in different building arrays under three incoming flow directions. Fig. 5 (a) - (f) demonstrates that under consistent building layout, wind speed, and wind direction, the concentration of bioaerosols in the lee area of buildings generally exceeds that in the street valley, particularly closer to the release source. This observation is primarily attributed to the presence of the leeward crosswind shadow zone.

Comparing Fig. 5 (a) and (g), it is evident that in the 3×5 arrays, the concentration of bioaerosols at spatial sampling points (P_1 , P_2 , and P_3) near the release source is lower on the lee side than in the street valley. The possible reason is that the buildings in the 3×5 arrays create a narrow channel that amplifies eddy currents on the lee side under strong airflow conditions, leading to a dilution of bioaerosol concentration (Zhang et al., 2020c). As the distance from the release source increases, Fig. 5 (a) and (c) reveal a decrease in bioaerosol concentration on both the lee side of buildings and in the street valley for the 3×3 arrays. This conclusion is corroborated by the findings in the literature (Liu et al., 2023a). Similarly, Fig. 5 (d) and (f) indicate a decreasing trend in bioaerosol concentration on the lee side of buildings, with a contrasting trend observed in the street valley for the 4×4 arrays. Fig. 5 (g) illustrates that bioaerosol concentration on the lee side of buildings exhibits an increasing trend in the 3×5 arrays, while the concentration in the street valley shows a decreasing trend. This result indicates that the building layout has a significant impact on bioaerosol dispersion. Furthermore, Fig. 5 demonstrates that under constant wind direction and speed, bioaerosol concentrations are lowest in the 4×4 arrays. This difference is likely attributed to the smaller spacing and more significant number of buildings in the 4×4 arrays, which enlarges the wind shadow area and increases deposition on building surfaces, thereby markedly reducing bioaerosol concentrations at spatial locations (Poppema et al., 2021).

As depicted in Fig. 5, under identical building layout and wind speed conditions, the incident wind direction predominantly influences the uniformity of bioaerosol concentration distribution and the migration trajectory of pollutants within the building array's spatial locations (Dai et al., 2024). For the same building layout and inbound wind direction, increasing wind speed will significantly reduce the concentration of bioaerosol in each spatial location, indicating that high wind speed is conducive to diluting pollutants in urban areas and improving outdoor air quality (Lee & Mak, 2021, Q. Zhao et al., 2024). However, excessive wind speed may compromise pedestrian comfort levels (Norouzias et al., 2022). Therefore, these factors should be taken into account in the planning and design of buildings, and the comfort level and health risk of pedestrians should be comprehensively evaluated. As illustrated in Figs. 5 (a) - (f), at a constant wind speed and a 45° wind direction, bioaerosol concentrations are lower across various building arrays. Notably, the 4×4 arrays configuration is more effective than the 3×3 arrays in diluting bioaerosol concentrations.

3.3. Health risks for various age levels

Studies have shown that varying breathing rates and physiological responses among different demographic groups result in distinct health risks associated with exposure to urban environments (Pasalari et al., 2019, Haas, 2015, Coccia, 2020). This study comprehensively assesses the health risks posed to individuals of various age groups under the influence of microclimate and building layout. The annual infection probability of people of different ages in different building arrays under the influence of microclimate is shown in Fig. 6. These specific results can be found in Supplementary Materials Tables 3-9. By comparing various exposure scenarios, it can be seen that the changing trend of health risks of people at different ages is similar, mainly as follows: adults face higher health risks compared to other demographics, while pre-kindergarten exhibits the lowest risks, with a disparity of approximately 2.56 times. This finding aligns with the conclusions drawn in the literature (Ali et al., 2022a). This discrepancy is primarily attributed to variations in respiratory rates across different age groups (see Table 3), alongside factors such as concentration levels and duration of exposure (Yan et al., 2024, Xu et al., 2021).

The bottom and top of the box respectively represent the first and third quartiles (25th and 75th percentile values), and the band inside the box denotes the second quartile (median). The bottom and top of the whiskers respectively represent the 5th (optimistic estimate at the best situation) and 95th (conservative estimate at the worst situation) percentile values. U.S. EPA = United States Environmental Protection Agency.

For the same age group, when the wind speed is U_{ref1} , the health risk of the population in each stage is higher than the U.S. EPA baseline. However, with increasing wind speeds up to U_{ref3} , health risks decrease across all age groups, with some stages meeting U.S. EPA benchmarks. Thus, increasing wind speed in each exposure scenario can significantly reduce health risks by an order of magnitude. The main reason was the decrease in concentration at each exposure scene, which was caused by the increase in wind speed (Zhao et al., 2024b). For the 3×3 arrays, comparing Figs. 6 (a), (b), and (c), it is evident that under the same airflow conditions, the wind direction does not influence the distribution pattern of health risks among different age groups. However, at a wind direction of 45° , a slight decrease in health risks compared to wind directions of 0° and 90° . It is noteworthy that this reduction trend diminishes with higher wind speeds. Similar observations can be made from Fig. 6 (d), (e), and (f). Under uniform microclimate conditions, the health risks for individuals of all ages in the 4×4 arrays are notably lower compared to other building layouts. This reason is primarily attributed to the smaller spacing and more significant number of buildings in the 4×4 array, resulting in lower levels of bioaerosols suspended in the air (Poppema et al., 2021).

The level of population health risk in urban environments hinges on factors such as bioaerosol exposure dose, respiratory rate, and risk characterization methods. However, our analysis shows that wind speed, wind direction, and building layout are also important factors influencing population health risk across various urban environments. In addition, it was found that reducing wind speed health risk was much more effective than adjusting building layout and wind direction. Exposure risks can be avoided by planning a reasonable building layout, strengthening outdoor ventilation and introducing appropriate wind angles.

The disease burden of pedestrians of various ages in different building arrays under the influence of microclimate is shown in Fig. 7 and Supplementary Materials Tables 10-16. Fig. 7 shows that under various exposure scenarios, the disease burden faced by adults is higher than that of other age groups, and the disease burden of infants is the lowest, with a difference of about 2.56 times. This conclusion is consistent with the findings of health risks in all age groups, indicating that the disease burden is closely related to health risks. However, the difference is that the disease burden faced by people of all ages in most

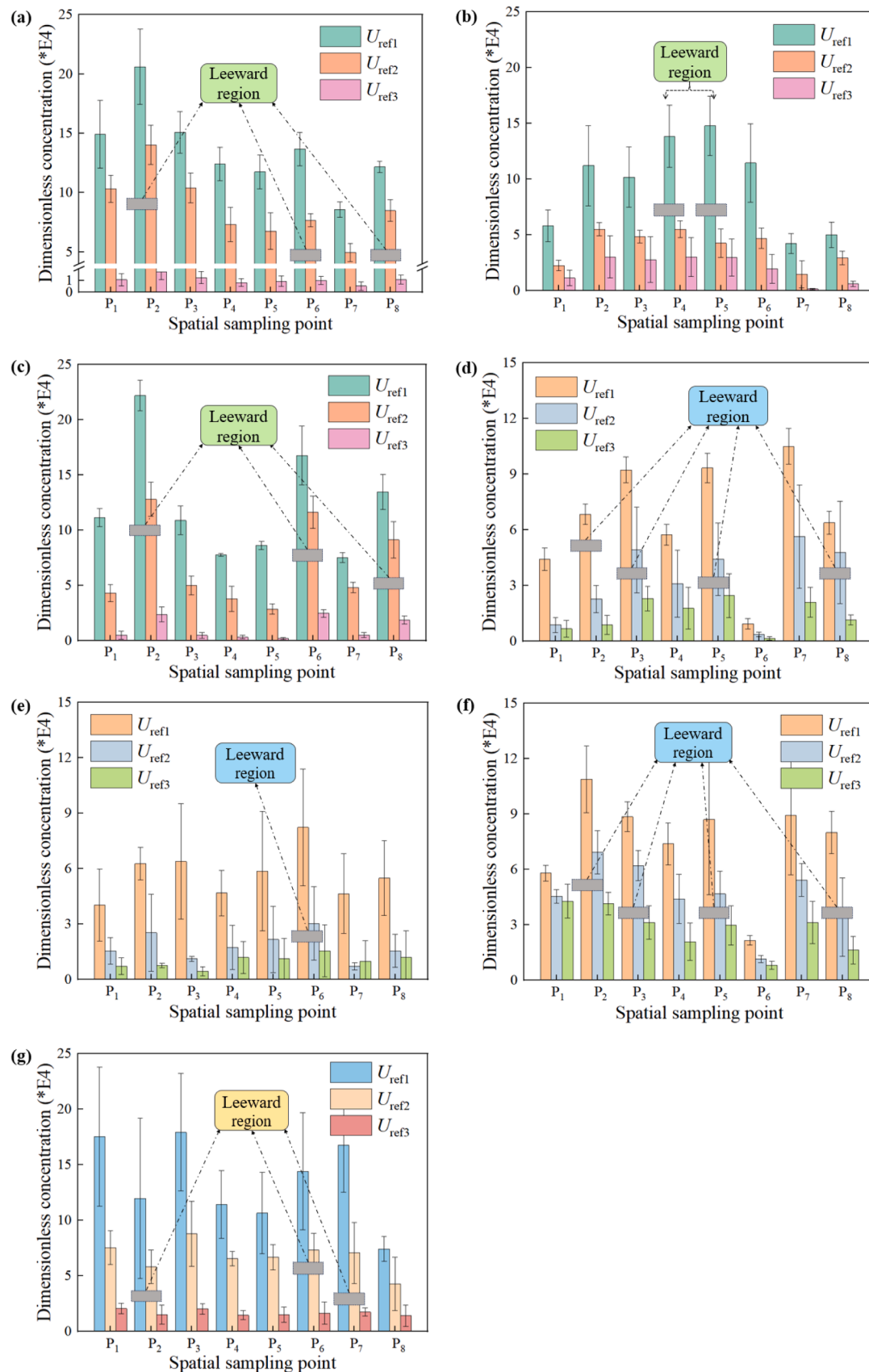


Fig. 5. The dimensionless concentration of bioaerosols within three parallel experiments at different spatial locations in different building arrays. (a) 3 × 3–0°; (b) 3 × 3–45°; (c) 3 × 3–90°; (d) 4 × 4–0°; (e) 4 × 4–45°; (f) 4 × 4–90°; (g) 3 × 5–0° The error bars represent the range of results from three parallel experiments.

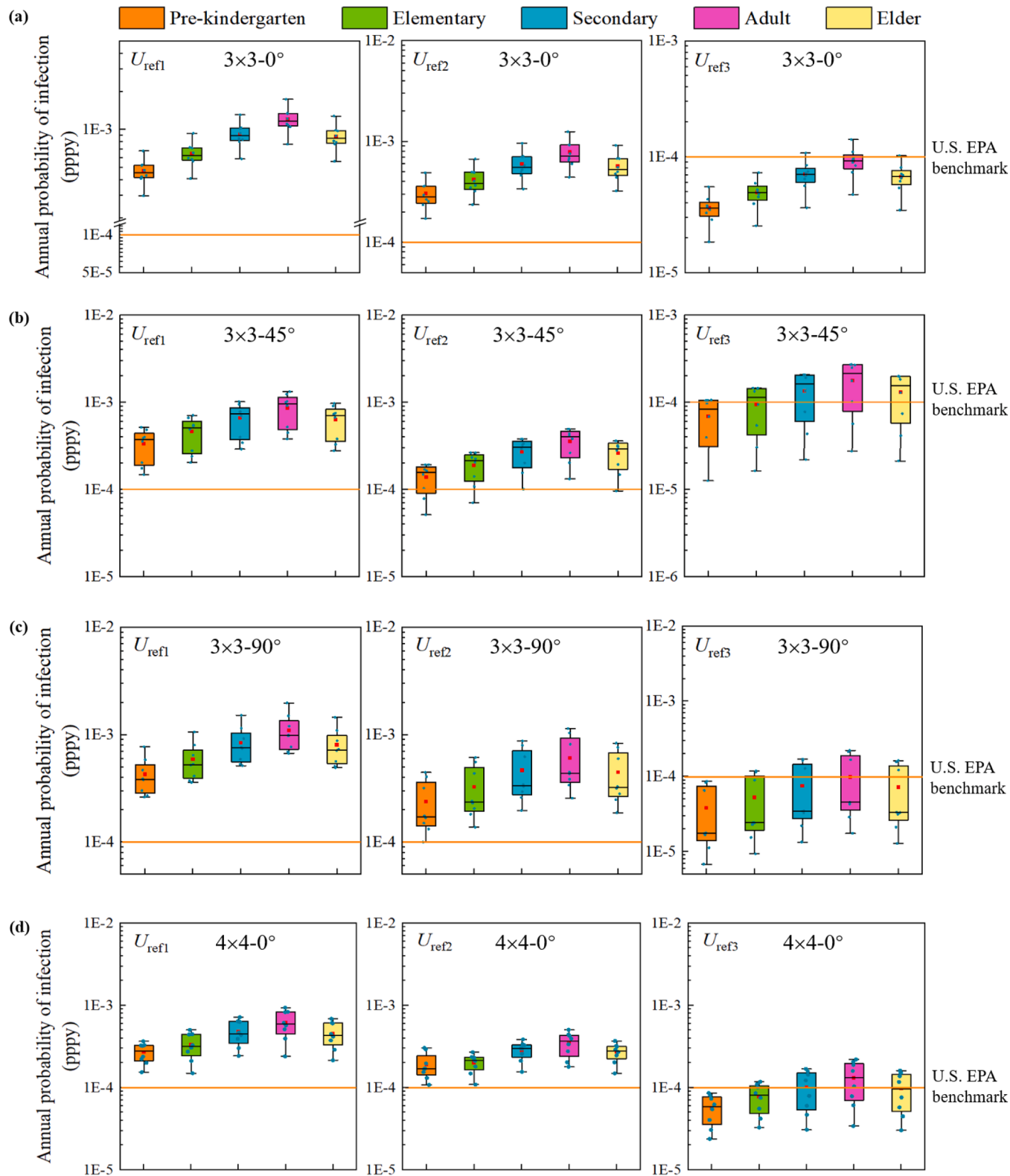


Fig. 6. Annual infection probability of pedestrians of various ages in different building arrays under the influence of microclimate. (a) $3 \times 3-0^\circ$; (b) $3 \times 3-45^\circ$; (c) $3 \times 3-90^\circ$; (d) $4 \times 4-0^\circ$; (e) $4 \times 4-45^\circ$; (f) $4 \times 4-90^\circ$; (g) $3 \times 5-0^\circ$

exposure scenarios is higher than the WHO standards. It can be seen from the side that the accidental release of bioaerosols in urban environments and bioterrorist attacks are inevitable for the health risks of people of all ages. It is of great significance to strengthen biological

prevention and control measures and explore the health risks of various populations under the influence of microclimate and building layout for urban biosafety prevention and control.

The bottom and top of the box respectively represent the first and

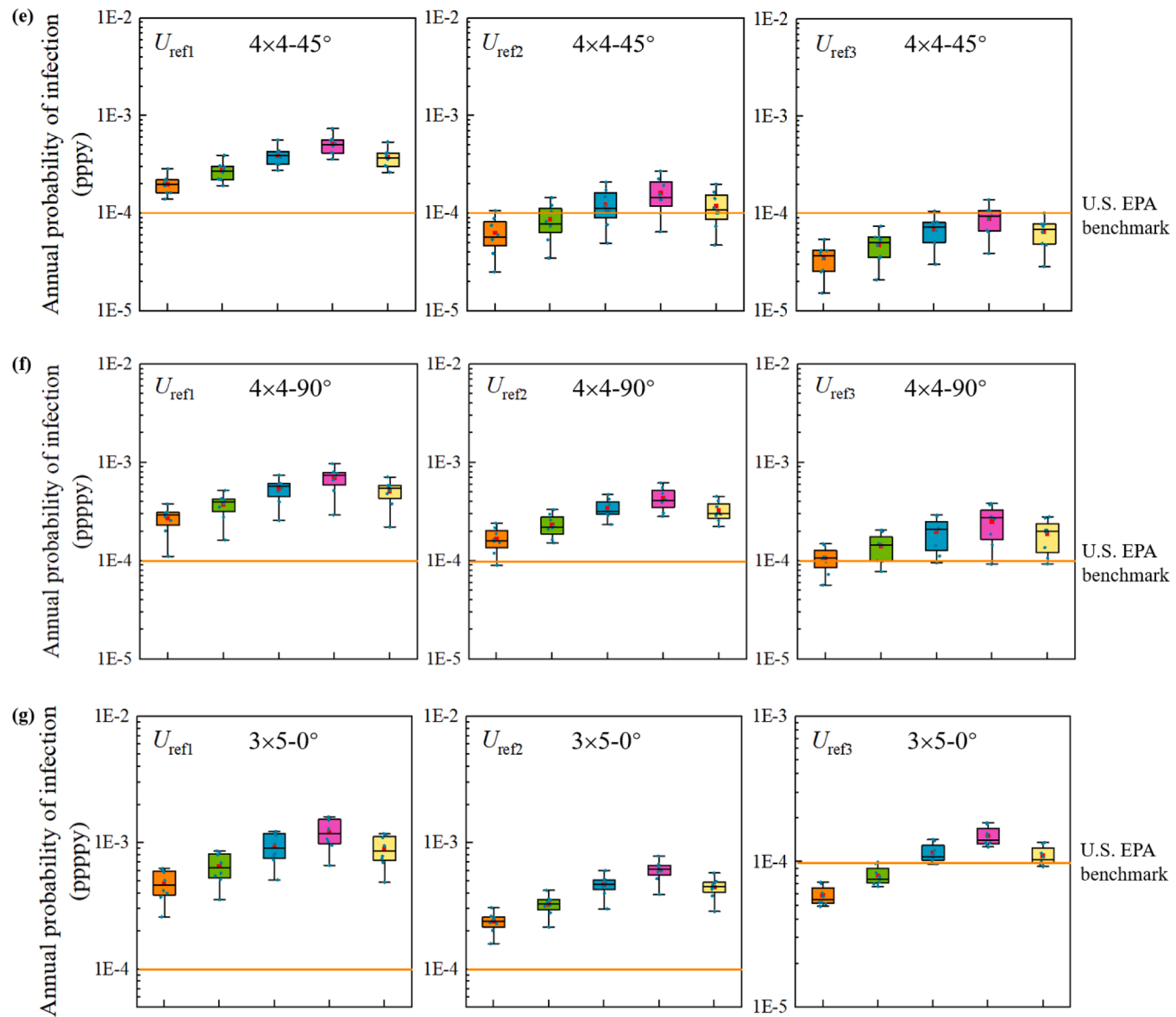


Fig. 6. (continued).

third quartiles (25th and 75th percentile values), and the band inside the box denotes the second quartile (median). The bottom and top of the whiskers respectively represent the 5th (optimistic estimate at the best situation) and 95th (conservative estimate at the worst situation) percentile values. WHO = World Health Organization.

Fig. 7 illustrates that irrespective of building layout and incoming direction. There is a marked decrease in disease burden across all age groups with increasing wind speed. In addition, the effects of wind direction and building layout on the disease burden of all age groups are similar to the impact on the annual infection probability. Notably, as depicted in Fig. 7, wind speed exhibits greater sensitivity than wind direction and building layout in influencing disease burden among people of all ages. These findings underscore the critical role of wind speed in mitigating the disease burden associated with bioaerosol exposure in urban environments. They highlight the importance of enhancing outdoor ventilation strategies and considering wind dynamics in urban planning to manage and reduce health risks across diverse population groups effectively.

3.4. Sensitivity analysis of microclimate and building layout to health risks

As depicted in Figs. 6 and 7, adults consistently exhibit the highest health risks (including annual probability of infection and disease burden) across all exposure scenarios among various age groups. Therefore, the subsequent analysis focuses on investigating the influence of microclimate factors and building a layout for health risks specifically for adults.

3.4.1. Impact of wind speed

The impact of wind speed on health risks in adults is shown in Fig. 8. As can be seen from Figs. 8 (a) - (c), when the wind speed increases from U_{ref1} to U_{ref3} , the annual infection probability at different spatial locations in 3×3 array decreases by 93.81 %, 96.18 % and 97.73 % at the three incoming directions of the incident wind angle of 0°, 45° and 90°, respectively (P_7). For the 4×4 arrays, the annual infection probability at different spatial locations decreased by at least 75.07, 74.49 and 61.76 percentage points in the three incoming directions of the wind angles of 0°, 45° and 90°. For the 3×5 arrays, at wind speed U_{ref1} , the

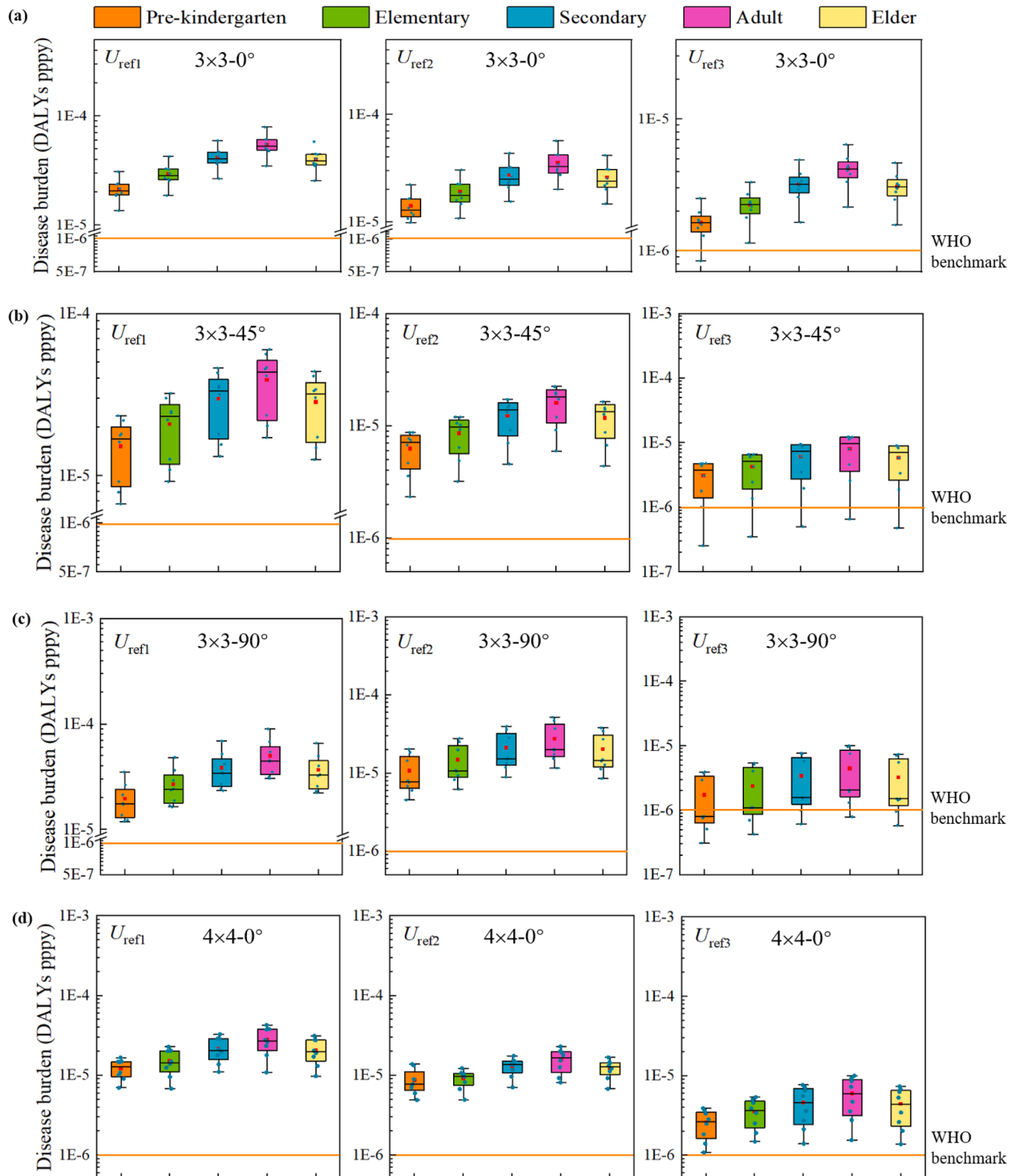


Fig. 7. Disease burden of pedestrians of various ages in different building arrays under the influence of microclimate. (a) $3 \times 3-0^\circ$; (b) $3 \times 3-45^\circ$; (c) $3 \times 3-90^\circ$; (d) $4 \times 4-0^\circ$; (e) $4 \times 4-45^\circ$; (f) $4 \times 4-90^\circ$; (g) $3 \times 5-0^\circ$

annual probability of infection ranged from 56.24 % to 65.59 % across various spatial locations; at U_{ref2} , it ranged from 27.64 % to 35.43 %; and at U_{ref3} , it varied from 6.83 % to 10.72 %. These results indicate a substantial reduction in the annual probability of infection across

different spatial locations with increasing wind speed, aligning well with findings in the literature (Gollakota et al., 2021, Mendell et al., 2024).

Fig. 8 (d) - (f) show that irrespective of building layout and incoming wind direction, increased wind speed results in a substantial reduction

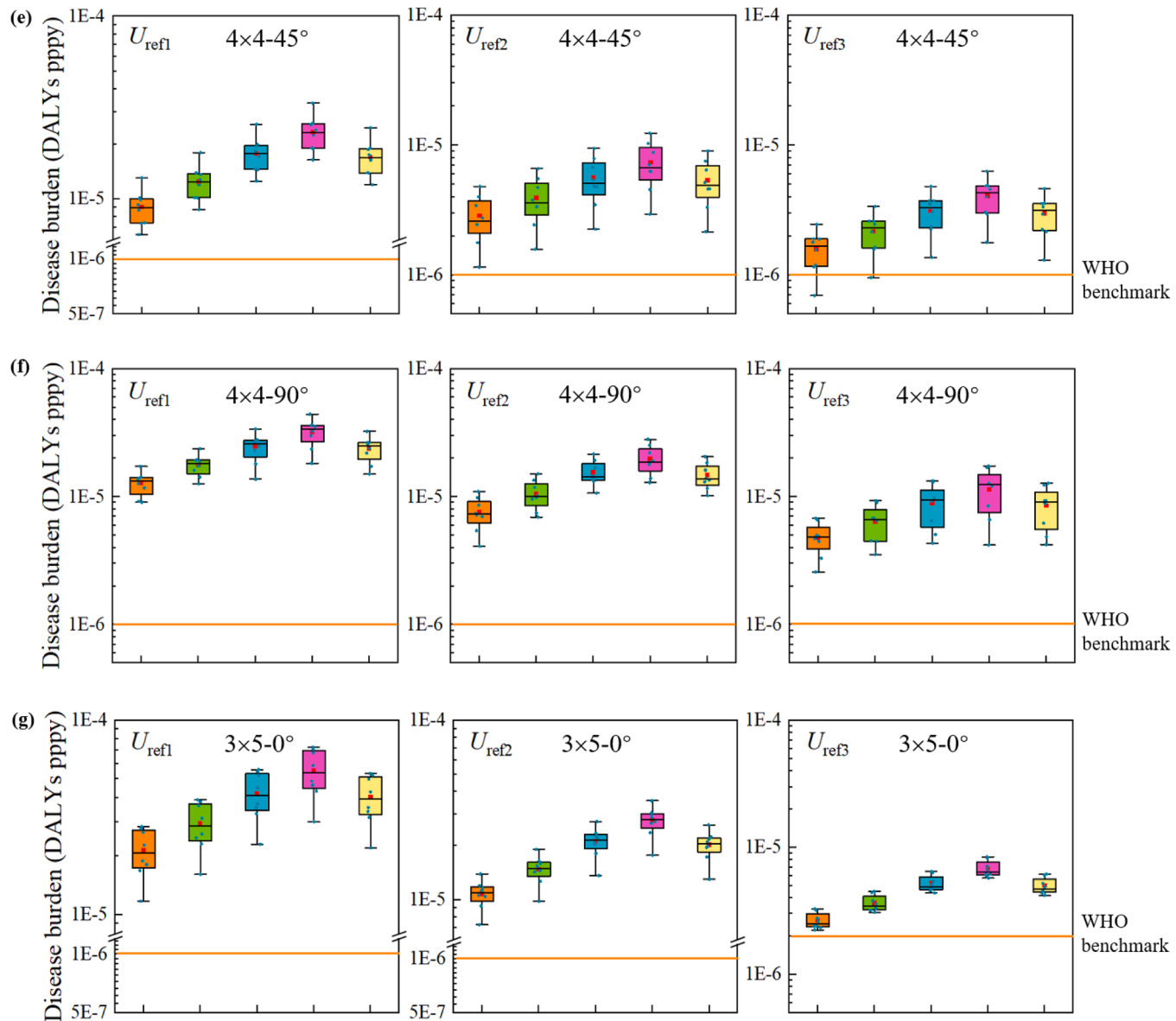


Fig. 7. (continued).

in disease burden by 1–2 orders of magnitude. This finding is consistent with the research by Coccia (Coccia, 2021). In the 3×3 arrays, as the wind speed increased from $U_{\text{ref}1}$ to $U_{\text{ref}3}$, the disease burden decreased by 93.81 %, 96.18 %, and 97.73 % at different spatial locations corresponding to wind angles of 0° , 45° , and 90° , respectively. Similarly, for the 4×4 arrays, the disease burden decreased by 87.16 %, 93.14 %, and 79.62 % at these respective wind angles. In the case of the 3×5 array, the maximum reduction in disease burden across different spatial locations was 89.57 %. The results show that proper ventilation can improve air quality in urban environments (Coccia, 2021, Hang et al., 2023). Moreover, it is noteworthy that the interaction between wind direction and speed, as well as the relationship between wind speed and building layout, also influences disease burden in urban environments to some extent.

3.4.2. Impact of wind direction

Fig. 9 shows the significant influence of wind direction on adult health risks. For the 3×3 arrays, when wind speeds are low, the annual infection probability is higher at wind angles of 0° and 90° compared to 45° . This disparity is likely due to slower wind speeds, which diminish

the dilution and dispersion effects of the airflow on bioaerosols. Consequently, bioaerosols remain within the building array for longer durations, increasing the annual infection probability at wind angles parallel (0°) and perpendicular (90°) to the flow direction relative to wind angle 45° . As wind speed increases to $U_{\text{ref}3}$, the annual infection probability at P₁-P₆ locations is higher at a wind angle of 45° compared to other incident wind angles (Fig. 9 (a)). The main reason is that the airflow becomes more intense as the wind speed increases, and the dispersion effect of pollutants is significantly enhanced (Zhao et al., 2024b). At a wind direction of 45° , bioaerosols are more uniformly distributed in space, as depicted in Fig. 5.

It is worth noting that when the wind speed changes, the incidence angles of 0° and 90° account for almost the same proportion of infection probabilities. The possible reason is that the 3×3 array is relatively regular, and the arrangement mode does not change, and changing the wind direction only changes the occluded area of the architectural complex in the direction of the incoming flow. For 4×4 array, except at spatial location P₆, the annual infection probability is relatively lower when the wind direction angle is 45° compared to wind angles of 0° and 90° .

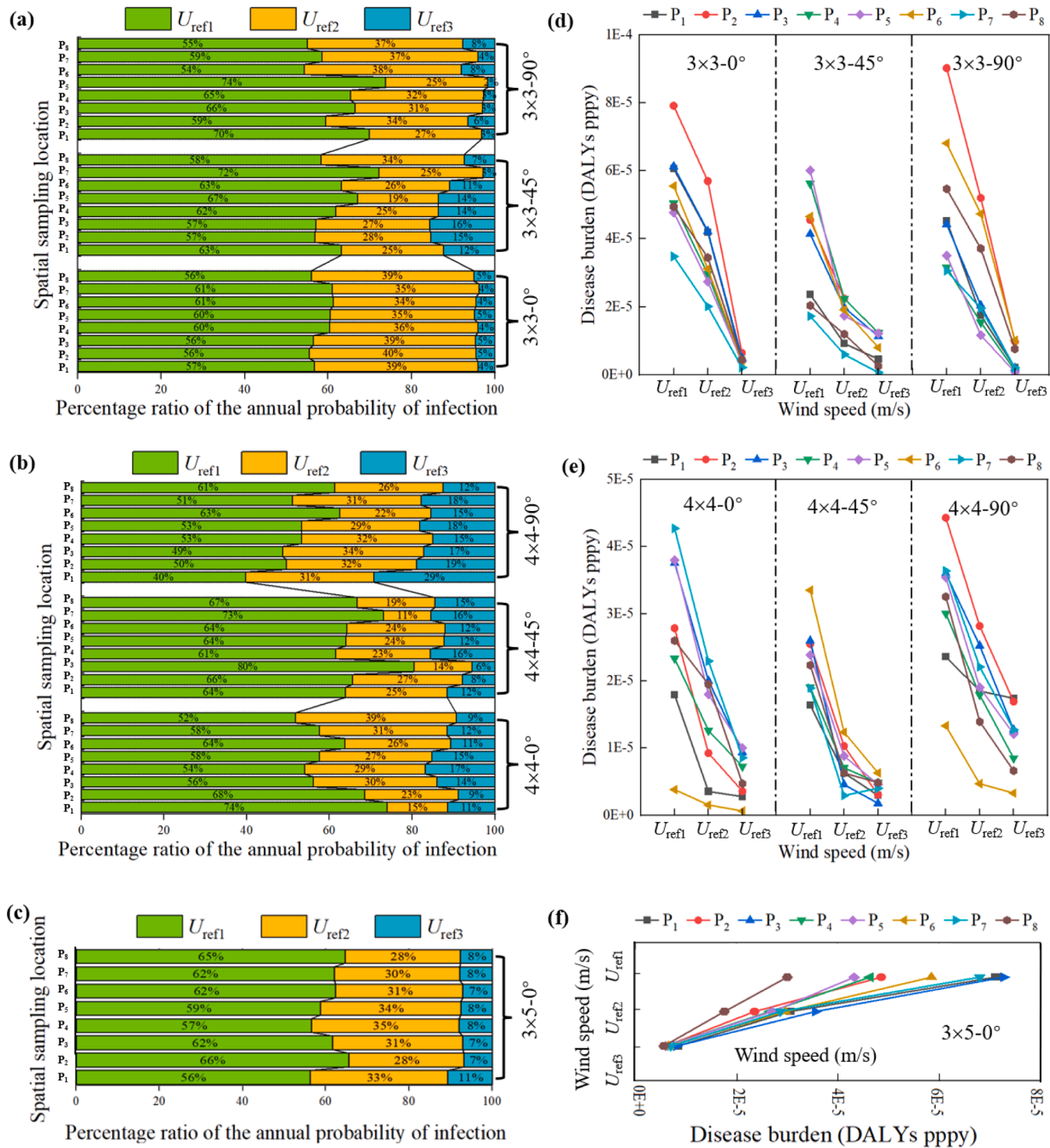


Fig. 8. Effect of wind speed on adult health risk. (a)-(c) represent the annual infection probability in 3×3 , 4×4 and 3×5 building arrays, respectively. (d)-(f) represent the disease burden in 3×3 , 4×4 and 3×5 building arrays, respectively.

Figs. 9 (c) and (d) depict the disease burden within 3×3 and 4×4 arrays, respectively. Across both building layouts, as the incident wind angle transitions from 0° to 45° to 90° , the disease burden at most spatial locations shows an initial decrease followed by an increase. This pattern closely correlates with the building layout and the incident wind angle (Pourteimouri et al., 2023). However, specific spatial locations deviate from this general trend, potentially due to varying airflow patterns influenced by building obstruction or wind flow interference (Liu et al., 2018), thereby impacting bioaerosol distribution and disease burden. In

addition, changes in wind speed may have complex interaction effects with changes in wind direction. Notably, the lower the wind speed, the smaller the difference in disease burden caused by the change in wind direction.

3.4.3. Impact of building layout

To investigate the impact of building layout on health risk, we examined the disease burden among adults at similar coordinate locations (locations A and B) within 3×3 , 4×4 , and 3×5 arrays, using a

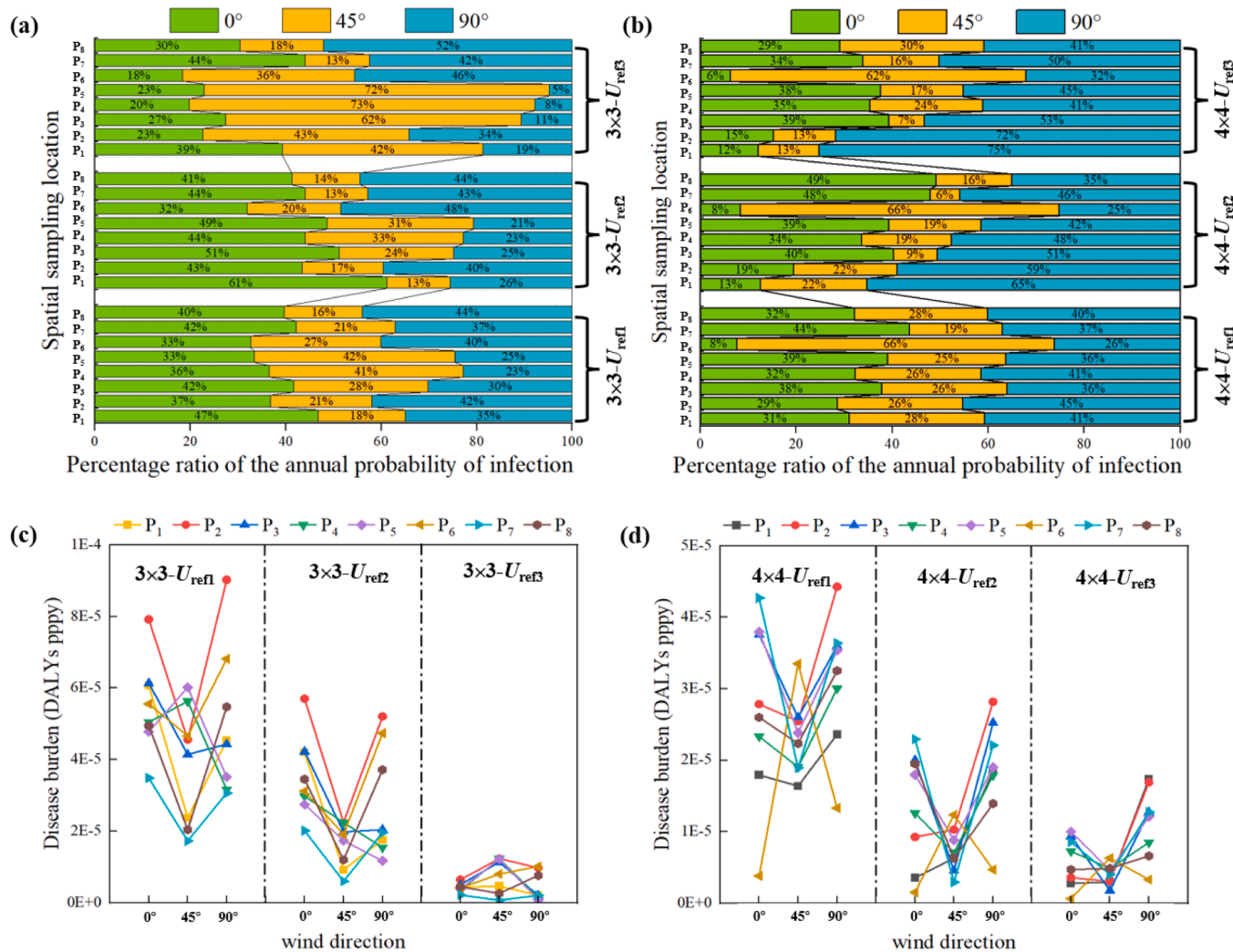


Fig. 9. Effect of wind direction on adult health risk. (a) and (b) represent the annual infection probability in 3×3 and 4×4 building arrays, respectively. (c) and (d) represent the disease burden in 3×3 and 4×4 building arrays, respectively.

wind angle of 0° as an example, as depicted in Fig. 10. Locations A and B correspond to sampling points P₂ and P₆ in the 3×3 and 3×5 arrays, and sampling points P₁ and P₄ in the 4×4 array, respectively. For the annual infection probability at locations A and B, when the wind speed was constant, the annual infection probability of adults at 4×4 array was the most minor, mainly due to the fact that adults at 4×4 array had the lowest exposure dose at locations A and B (see Fig. 5). Studies have shown that dense building layouts can hinder the development of airflow, leading to the accumulation of pollutants between buildings, and thus increase the burden of diseases (Liang & Gong, 2020). Although the 4×4 arrays is more densely laid out than other architectural arrays, locations A and B are situated within street valleys, and the bioaerosol is transported to a further area under the action of airflow.

In the 3×3 arrays, the annual infection probability at locations A and B was higher than that at the 3×5 arrays. However, with the increase in wind speed, the bioaerosol migration was promoted under the action of strong airflow, resulting in a smaller gap (Fig. 10 (c)). Fig. 10 illustrates that within the 3×3 and 3×5 arrays, location A consistently exhibits higher annual infection probabilities compared to location B. It can be seen that the disease burden of the lee side decreases with the increase of distance, mainly due to the decrease of bioaerosol concentration with the increase of distance (Liu et al., 2023b). Conversely, in the 4×4 arrays, where both locations A and B are situated within street valleys, the annual infection probability of location B is higher than that

of location A under the action of airflow. These findings suggest that a reasonable building layout can effectively mitigate health risks and enhance the quality of living.

3.5. Limitation and future research

This study relies on wind tunnel experiments and idealized urban models, which impose limitations on capturing the full complexity of bioaerosol behavior. Notably, the effects of temperature and humidity fluctuations on the aerodynamic migration of bioaerosols were not systematically examined due to these experimental constraints. Future research should encompass a broader range of environmental conditions, including varying temperature and humidity levels, and utilize more realistic urban environments, such as through outdoor scaling experiments. Additionally, further investigation into bioaerosol resuspension and mass flow transport under high wind speeds is warranted. Enhancing experimental methods and practical validation is crucial for advancing biosafety strategies and optimizing urban planning to address bioaerosol-related health risks comprehensively.

4. Conclusions

This study examines the impact of microclimate and building layout on bioaerosol aerodynamic characteristics in urban environments

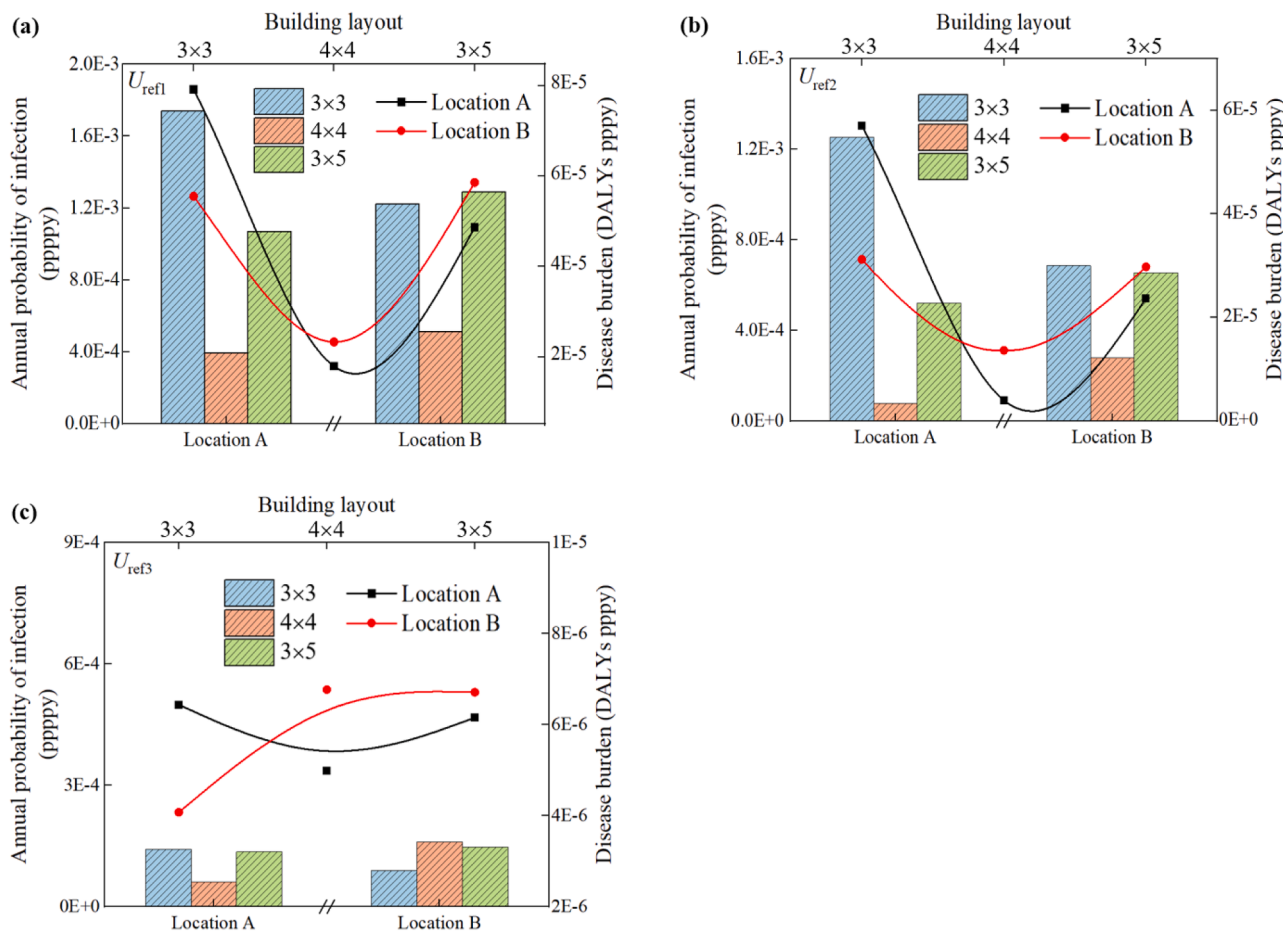


Fig. 10. Effects of building layout on adult infection probability and disease burden. (a) U_{ref1} ; (b) U_{ref2} ; (c) U_{ref3} . Location A refers to spatial sampling positions P_2 , P_1 and P_2 in 3×3 , 4×4 and 3×5 building arrays, respectively. Location B respective refers to spatial sampling positions P_6 , P_4 and P_6 in 3×3 , 4×4 and 3×5 building arrays.

through wind tunnel experiments and idealized urban scale models. Quantitative microbiological risk assessment methods were employed to evaluate health risks across different age groups. In addition, the sensitivity of microclimate and building layout to health risks is also explored. As the distance from the release source increases, bioaerosol concentrations on the leeward side of buildings in both 3×3 and 4×4 arrays decrease, whereas concentrations in the 3×5 arrays increase. Compared to the 3×3 and 3×5 arrays, the 4×4 arrays exhibit relatively lower bioaerosol concentrations under specific wind directions and speeds. The incident wind direction primarily influences the uniformity of bioaerosol concentration distribution and pollutant migration trajectories within the building array. For a given building layout and wind direction, increasing the wind speed from 1.36 to 2.54 m/s significantly reduces bioaerosol concentrations across various spatial locations within different arrays. Additionally, for the same building layout and wind speed, bioaerosol concentrations are lower when the incident wind direction is at 45° .

The health risk of adults was higher than that of other groups, and the health risk of pre-kindergarten was the lowest. The difference between the two was about 2.56 times. Increased wind speed from 1.36 to 2.54 m/s markedly reduces infection probabilities and disease burden by 1–2 orders of magnitude, particularly in dense building layouts. Wind direction also affects the uniformity and migration trajectory of bioaerosol distribution, with a 45° angle promoting more uniform aerosol dispersion and reduced health risks, especially at higher wind speeds. Bioaerosol concentrations are generally higher on the leeward side of buildings compared to street valleys, with significant variability in airflow among different building arrangements. Wind speed exerts a

more pronounced effect on health risks than building layout or wind direction.

Urban planning should aim to increase wind speeds by incorporating air ducts and green spaces to enhance pollutant dilution and diffusion. Ensuring that incoming air is directed at a certain tilt Angle (45° angle) to avoid aerosol accumulation in building leeward areas is crucial. Additionally, reducing building density, increasing spacing, and designing spacious streets and open regions can further improve airflow and pollutant dispersion. Particular attention should be given to minimizing health risks for young pre-kindergarten and adults. Optimizing wind speed, direction, and building layout will contribute to better urban air quality and reduce bioaerosol-related health risks.

CRediT authorship contribution statement

Zhijian Dong: Writing – review & editing, Writing – original draft, Investigation, Formal analysis, Data curation, Conceptualization. **Zhijian Liu:** Writing – review & editing, Funding acquisition, Formal analysis, Data curation, Conceptualization. **Chenxing Hu:** Writing – review & editing, Investigation, Formal analysis, Data curation. **Chenglin Ye:** Writing – review & editing, Formal analysis. **Yongjun Jin:** Writing – review & editing, Investigation, Formal analysis. **Haiyang Liu:** Investigation, Data curation. **Rui Rong:** Writing – review & editing, Software. **Yuchen He:** Investigation, Data curation. **Li Chen:** Validation, Software. **Chuanchen Li:** Methodology, Investigation. **Yaolong Shi:** Methodology, Investigation. **Yufeng Su:** Investigation.

Declaration of competing interest

The authors declare that they have no known competing financial interests or personal relationships that could have appeared to influence the work reported in this paper.

Acknowledgements

This work was funded by the National Natural Science Foundation of China (No. 42122058), the Outstanding Youth Team Project Fund (2752023YQ001), the Distinguished Youth Science Foundation of Hebei Province (No. E2023502015), the National Natural Science Foundation of China (No. 41977368).

Supplementary materials

Supplementary material associated with this article can be found, in the online version, at [doi:10.1016/j.scs.2024.106098](https://doi.org/10.1016/j.scs.2024.106098).

Data availability

Data will be made available on request.

References

- Abohela, I., Hamza, N., & Dudek, S. (2013). Effect of roof shape, wind direction, building height and urban configuration on the energy yield and positioning of roof mounted wind turbines. *Renewable Energy*, 50, 1106–1118.
- Ali, W., An, D.-Z., Yang, Y.-F., Cui, B.-B., Ma, J.-X., Zhu, H., Li, M., Ai, X.-J., & Yan, C. (2022a). Comparing bioaerosol emission after flushing in squat and bidet toilets: Quantitative microbial risk assessment for defecation and hand washing postures. *Building and Environment*, 221, Article 109284.
- Ali, W., Yang, Y.-F., Gong, L., Yan, C., & Cui, B.-B. (2022b). Emission characteristics and quantitative health risk assessment of bioaerosols in an indoor toilet after flushing under various ventilation scenarios. *Building and Environment*, 207, Article 108463.
- Baş, H., Andrianne, T., & Reiter, S. (2024). City configurations to optimise pedestrian level ventilation and wind comfort. *Sustainable Cities and Society*, 114, Article 105745.
- Bendjabbar, H., Abdellah-ElHadj, A., & Abbas, M. (2016). Full-scale, wind tunnel and CFD analysis methods of wind loads on heliostats: A review. *Renewable and Sustainable Energy Reviews*, 54, 452–472.
- Bezabeh, M. A., Bitsuamlak, G. T., Popovski, M., & Tesfamariam, S. (2018). Probabilistic serviceability-performance assessment of tall mass-timber buildings subjected to stochastic wind loads: Part I - structural design and wind tunnel testing. *Journal of Wind Engineering and Industrial Aerodynamics*, 181, 85–103.
- Blocken, B., Stathopoulos, T., & van Beeck, J. P. A. J. (2016). Pedestrian-level wind conditions around buildings: Review of wind-tunnel and CFD techniques and their accuracy for wind comfort assessment. *Building and Environment*, 100, 50–81.
- Bouketta, S., & Bouchahm, Y. (2020). Numerical evaluation of urban geometry's control of wind movements in outdoor spaces during winter period. Case of Mediterranean climate. *Renewable Energy*, 146, 1062–1069.
- Chen, G., Hang, J., Chen, L., & Lin, Y. (2023). Comparison of uniform and non-uniform surface heating effects on in-canyon airflow and ventilation by CFD simulations and scaled outdoor experiments. *Building and Environment*, 244, Article 110744.
- Coccia, M. (2020). An index to quantify environmental risk of exposure to future epidemics of the COVID-19 and similar viral agents: Theory and practice. *Environmental Research*, 191, Article 110155.
- Coccia, M. (2021). How do low wind speeds and high levels of air pollution support the spread of COVID-19? *Atmospheric Pollution Research*, 12, 437–445.
- Cui, P.-Y., Zhang, Y., Chen, W.-Q., Zhang, J.-H., Luo, Y., & Huang, Y.-D. (2021). Wind-tunnel studies on the characteristics of indoor/outdoor airflow and pollutant exchange in a building cluster. *Journal of Wind Engineering and Industrial Aerodynamics*, 214, Article 104645.
- Dai, T., Liu, S., Liu, J., Jiang, N., & Chen, Q. (2024). Quantifying the uncertainty of the effects of varying wind conditions on outdoor airflow and pollutant dispersion, 113. *Sustainable Cities and Society*, Article 105698.
- de Ondarza, J. (2017). Ozone Sensitivity and Catalase Activity in Pigmented and Non-Pigmented Strains of *Serratia Marcescens*. *The open microbiology journal*, 11, 12–22.
- Devleesschauwer, B., Havelaar, A. H., Maertens de Noordhout, C., Haagsma, J. A., Praet, N., Dorni, P., Duchateau, L., Torgerson, P. R., Van Oyen, H., & Speybroeck, N. (2014). Calculating disability-adjusted life years to quantify burden of disease. *International journal of public health*, 59, 565–569.
- Dong, Z., Liu, Z., Hu, C., Jin, Y., Ye, C., He, Y., & Rong, R. (2024). Modeling the long-range transmission of airborne bioaerosol releases in a high-density urban environment, 55. *Urban Climate*, Article 101883.
- Duan, C., Wang, Y., Wang, Q., Li, J., Xie, J., Liu, S., Yang, J., Huang, Y., Zhao, W., & Yin, W. (2023). Gram-negative bacterial infection causes aggravated innate immune response in sepsis: Studies from clinical samples and cellular models. *Biochemical and Biophysical Research Communications*, 650, 137–144.
- Fatemi, M., & Jebali, A. (2022). Path analysis of the effect of climatic elements on wind speed and desertification progress in Central Iran. *Arabian Journal of Geosciences*, 15, 930.
- Frączek, K., Rozycki, H. J., Ropke, D. R. J. E. C., & E, S (2014). *Statistical Analyses of Bioaerosol Concentration at Municipal Landfill Site*, 21, 229–243.
- Gao, T., Wang, W., Ma, J., Zheng, T., & Li, L. (2024). Diffusion behavior and transport risk of bioaerosol particles in a domestic waste landfill site in an arid and cold region of northwestern China. *Journal of Hazardous Materials*, 479, Article 135629.
- Gollakota, A. R. K., Gautam, S., Santosh, M., Sudan, H. A., Gandhi, R., Sam Jebadurai, V., & Shu, C.-M. (2021). *Bioaerosols: characterization, pathways, sampling strategies, and challenges to geo-environment and health*, 99 pp. 178–203. Gondwana Research.
- Gonzales-Gustavson, E., Rusiñol, M., Medema, G., Calvo, M., & Girones, R. (2019). Quantitative risk assessment of norovirus and adenovirus for the use of reclaimed water to irrigate lettuce in Catalonia. *Water Research*, 153, 91–99.
- Guo, Z., Zhang, X., Wu, J., Yu, J., Xu, M., Chen, D., Zhang, Z., Li, X., Chi, Y., & Wan, S. (2020). In vitro inhibitory effect of the bacterium *Serratia marcescens* on *Fusarium* proliferatum growth and fumonisins production. *Biological Control*, 143, Article 104188.
- Haas, C. N. (2015). Microbial dose response modeling: past, present, and future. *Environ Sci Technol*, 49, 1245–1259.
- Hang, J., & Chen, G. (2022). *Experimental study of urban microclimate on scaled street canyons with various aspect ratios*, 46. Urban Climate, Article 101299.
- Hang, J., Wang, X., Liang, J., Zhang, X., Wu, L., Du, Y., Zhang, Y., & Buccolieri, R. (2023). Numerical investigation of the impact of urban trees on O3–NOx–VOCs chemistry and pollutant dispersion in a typical street canyon. *Atmospheric Environment*, 311, Article 119998.
- Havelaar, A. H., Kirk, M. D., Torgerson, P. R., Gibb, H. J., Hald, T., Lake, R. J., Praet, N., Bellinger, D. C., de Silva, N. R., Gargouri, N., Speybroeck, N., Cawthorne, A., Mathers, C., Stein, C., Angulo, F. J., Devleesschauwer, B., Adegoke, G. O., Afshari, R., Alasfoor, D., Baines, J., Balakrishnan, K., Hamza, W. M. B., Black, R. E., Bolger, P. M., Chaicumpla, W., Cravioto, A., Döpfer, D., Ehiri, J. E., Fazil, A., Ferreccio, C., Fèvre, E. M., Hall, G., Kasuga, F., Keddy, K. H., Lanata, C. F., Lei, H., Liu, X., Manyindo, B., Nasinyama, G., Ongolo-Zogo, P., Pitt, J. I., Rokni, M. B., Sripa, B., van Leeuwen, R., Verger, P., Willingham, A. L., Zhou, X. N., Aspinall, W., Buchanan, R., Budke, C., Caipo, M. L., Carabin, H., Cole, D., Cooke, R. M., Crump, J. A., El-Jardali, F., Fischer-Walker, C., Fürst, T., Haagsma, J. A., Hall, A. J., Henao, O., Hoffmann, S., Jensen, H., Jessani, N., Koopmans, M. P. G., Levine, M. M., de Noordhout, C. M., Majowicz, S., McDonald, S. A., Pires, S., Scallan, E., Sripa, B., Thomas, M. K., Verhoef, L., Wu, F., & Zeilmaker, M. (2015). World Health Organization Global Estimates and Regional Comparisons of the Burden of Foodborne Disease in 2010. *PLoS Medicine*, 12.
- Huertas, J. I., Martinez, D. S., & Prato, D. F. (2021). Numerical approximation to the effects of the atmospheric stability conditions on the dispersion of pollutants over flat areas. *Scientific Reports*, 11, 11566.
- Irda Sari, S. Y., Sunjaya, D. K., Shimizu-Furusawa, H., Watanabe, C., & Raksanagara, A. S. (2018). Water sources quality in urban slum settlement along the contaminated river basin in indonesia: Application of quantitative microbial risk assessment. *Journal of environmental and public health*, Article 3806537, 2018.
- Islam, A., Hasanuzzaman, M., Shammi, M., Salam, R., Bodrud-Doza, M., Rahman, M. M., Mannan, M. A., & Huq, S. (2021). Are meteorological factors enhancing COVID-19 transmission in Bangladesh? Novel findings from a compound Poisson generalized linear modeling approach. *Environmental science and pollution research international*, 28, 11245–11258.
- Keshavarzian, E., Jin, R., Dong, K., & Kwok, K. C. S. (2021). Effect of building cross-section shape on air pollutant dispersion around buildings. *Building and Environment*, 197, Article 107861.
- Khattak, A., Chan, P.-W., Chen, F., & Peng, H. (2023). Estimating turbulence intensity along the glide path using wind tunnel experiments combined with interpretable tree-based machine learning algorithms. *Building and Environment*, 239, Article 110385.
- Ledo, L., Kosasih, P. B., & Cooper, P. (2011). Roof mounting site analysis for micro-wind turbines. *Renewable Energy*, 36, 1379–1391.
- Lee, K. Y., & Mak, C. M. (2019). *A comprehensive approach to study stack emissions from a research building in a small urban setting*, 51. *Sustainable Cities and Society*, Article 101710.
- Lee, K. Y., & Mak, C. M. (2021). Effects of wind direction and building array arrangement on airflow and contaminant distributions in the central space of buildings. *Building and Environment*, 205, Article 108234.
- Li, C., & Tang, H. (2022). Comparison of COVID-19 infection risks through aerosol transmission in supermarkets and small shops. *Sustainable Cities and Society*, 76, Article 103424.
- Liang, L., & Gong, P. (2020). Urban and air pollution: a multi-city study of long-term effects of urban landscape patterns on air quality trends. *Scientific Reports*, 10, 18618.
- Liang, Z., Yu, Y., Wang, X., Liao, W., Li, G., & An, T. (2023). The exposure risks associated with pathogens and antibiotic resistance genes in bioaerosol from municipal landfill and surrounding area. *Journal of Environmental Sciences*, 129, 90–103.
- Lin, X., Fu, Y., Peng, D. Z., Liu, C.-H., Chu, M., Chen, Z., Yang, F., Tse, T. K. T., Li, C. Y., & Feng, X. (2024). *CFD- and BPNN-based investigation and prediction of air pollutant dispersion in urban environment*, 100. *Sustainable Cities and Society*, Article 105029.
- Liu, S., Pan, W., Zhao, X., Zhang, H., Cheng, X., Long, Z., & Chen, Q. (2018). Influence of surrounding buildings on wind flow around a building predicted by CFD simulations. *Building and Environment*, 140, 1–10.

- Liu, Z., Cao, H., Hu, C., Wu, M., Zhang, S., He, J., & Jiang, C. (2023a). Modeling the infection risk and emergency evacuation from bioaerosol leakage around an urban vaccine factory. *npj Climate and Atmospheric Science*, 6, 6.
- Liu, Z., Li, H., Chu, J., Huang, Z., Xiao, X., Wang, Y., & He, J. (2023b). The impact of high background particle concentration on the spatiotemporal distribution of *Serratia marcescens* bioaerosol. *Journal of Hazardous Materials*, 458, Article 131863.
- Liu, H., Ma, T., Liu, Z., Li, Q., Shen, B., Xin, J., Feng, C., Liu, M., & Liu, L. (2023c). Quantitative risk assessment for bacterial community in residential kitchens. *Building and Environment*, 228, Article 109841.
- Liu, Z., Hu, L., Hu, C., Liu, Q., Liang, Z., Rong, R., & Liu, H. (2023d). Aggravated exposure risks of children to multipath transmitted pathogens in indoor environments. *iScience*, 26, Article 108433.
- Luo, L., & Qi, C. (2021). An analysis of the crucial indicators impacting the risk of terrorist attacks: A predictive perspective. *Safety Science*, 144, Article 105442.
- Maing, M. (2022). Superblock transformation in Seoul Megacity: Effects of block densification on urban ventilation patterns. *Landscape and Urban Planning*, 222, Article 104401.
- Mendell, M. J., Chen, W., Ranasinghe, D. R., Castorina, R., & Kumagai, K. (2024). Carbon dioxide guidelines for indoor air quality: a review. *Journal of Exposure Science & Environmental Epidemiology*.
- Meselson, M., Guillemin, J., Hugh-Jones, M., Langmuir, A., Popova, I., Shelokov, A., & Yampolskaya, O. (1994). *The Sverdlovsk Anthrax Outbreak of 1979*, 266, 1202–1208.
- Miller, D., King, M. F., Nally, J., Drodge, J. R., Reeves, G. I., Bate, A. M., Cooper, H., Dalrymple, U., Hall, I., López-García, M., Parker, S. T., & Noakes, C. J. (2022). Modeling the factors that influence exposure to SARS-CoV-2 on a subway train carriage. *Indoor Air*, 32.
- Morawska, L., Buonanno, G., Mikszewski, A., & Stabile, L. (2022). The physics of respiratory particle generation, fate in the air, and inhalation. *Nature Reviews Physics*, 4, 723–734.
- Nielsen, P. V. (2009). Control of airborne infectious diseases in ventilated spaces. *Journal of the Royal Society, Interface*, 6(Suppl 6), S747–S755.
- Norouzian, A., Pilehchi Ha, P., Ahmadi, M., & Rijal, H. B. (2022). Evaluation of urban form influence on pedestrians' wind comfort. *Building and Environment*, 224, Article 109522.
- Ouyang, L., Yang, Y., Wu, Z., Jiang, Q., & Qiao, R. (2024). Towards inclusive urbanism: an examination of urban environment strategies for enhancing social equity in chengdu's housing zones. *Sustainable Cities and Society*, Article 105414.
- Pasalar, H., Ataei-Pirkooch, A., Aminikhah, M., Jafari, A. J., & Farzadkia, M. (2019). Assessment of airborne enteric viruses emitted from wastewater treatment plant: Atmospheric dispersion model, quantitative microbial risk assessment, disease burden. *Environmental Pollution*, 253, 464–473.
- Perez, V., Mena, K. D., Watson, H. N., Prater, R. B., & McIntyre, J. L. (2015). Evaluation and quantitative microbial risk assessment of a unique antimicrobial agent for hospital surface treatment. *American Journal of Infection Control*, 43, 1201–1207.
- Peterka, J. A., Meroney, R. N., & Kothari, K. M. (1985). Wind flow patterns about buildings. *Journal of Wind Engineering and Industrial Aerodynamics*, 21, 21–38.
- Poppema, D. W., Wijnberg, K. M., Mulder, J. P. M., Vos, S. E., & Hulscher, S. J. M. H. (2021). The effect of building geometry on the size of aeolian deposition patterns: Scale model experiments at the beach. *Coastal Engineering*, 168, Article 103866.
- Pourteimouri, P., Campmans, G. H. P., Wijnberg, K. M., & Hulscher, S. J. M. H. (2023). How wind direction and building spacing influences airflow patterns and sediment transport patterns around a row of beach buildings: a numerical study, 61. *Aeolian Research*, Article 100867.
- Qiao, Z., Wang, N., Chen, J., He, T., Xu, X., Liu, L., Sun, Z., & Han, D. (2023). Urbanization accelerates urban warming by changing wind speed: Evidence from China based on 2421 meteorological stations from 1978 to 2017. *Environmental Impact Assessment Review*, 102, Article 107189.
- Ryan, M. O., Haas, C. N., Gurian, P. L., Gerba, C. P., Panzl, B. M., & Rose, J. B. (2014). Application of quantitative microbial risk assessment for selection of microbial reduction targets for hard surface disinfectants. *American Journal of Infection Control*, 42, 1165–1172.
- Salunkhe, A. R., Dudhwadkar, S., Raju, N. P., & Tandon, S. (2024). Public health risk assessment and speciation of air-borne microorganisms in an office building. *Journal of Aerosol Science*, 179, Article 106362.
- Shi, K.-W., Wang, C.-W., & Jiang, S. C. (2018). Quantitative microbial risk assessment of Greywater on-site reuse. *Science of The Total Environment*, 635, 1507–1519.
- Smith, D. J., Jaffe, D. A., Birmele, M. N., Griffin, D. W., Schuerger, A. C., Hee, J., & Roberts, M. S. (2012). Free tropospheric transport of microorganisms from asia to north america. *Microbial Ecology*, 64, 973–985.
- Teng, X., Zhang, Y., Fan, Y., & Ge, J. (2024). Flow patterns and heat transfer of an idealized square city in non-uniform heat flux and different background wind conditions. *Building and Environment*, 262, Article 111779.
- Tin, D., Sabeti, P., & Ciottone, G. R. (2022). Bioterrorism: An analysis of biological agents used in terrorist events. *The American Journal of Emergency Medicine*, 54, 117–121.
- Tominaga, Y., & Stathopoulos, T. (2013). CFD simulation of near-field pollutant dispersion in the urban environment: A review of current modeling techniques. *Atmospheric Environment*, 79, 716–730.
- Xiao, Q., Fan, X., Guo, Y., Li, S., He, W., Deng, Y., Xiao, Z., Wang, P., & Wu, C. (2024). Tree form characteristics as criteria for tree species selection to improve pedestrian thermal comfort in street canyons: case study of a humid subtropical city, 105. *Sustainable Cities and Society*, Article 105339.
- Xie, W., Li, Y., Bai, W., Hou, J., Ma, T., Zeng, X., Zhang, L., & An, T. (2020). The source and transport of bioaerosols in the air: A review. *Frontiers of Environmental Science & Engineering*, 15, 44.
- Xie, Z., Xie, Y., Cao, B., & Zhu, Y. (2023). A study of the characteristics of dynamic incoming flow directions of different airflows and their influence on wind comfort. *Building and Environment*, 245, Article 110861.
- Xu, Y., Cai, J., Li, S., He, Q., & Zhu, S. (2021). *Airborne infection risks of SARS-CoV-2 in U.S. schools and impacts of different intervention strategies*, 74. *Sustainable Cities and Society*, Article 103188.
- Xu, X., Wang, C., Wang, P., Chu, Y., Guo, J., Bo, X., & Lin, A. (2023). Bioaerosol dispersion and environmental risk simulation: Method and a case study for a biopharmaceutical plant of Gansu province. *Science of The Total Environment*, 860, Article 160506.
- Xu, Y., Yang, J., Zheng, Y., & Li, W. (2024). Impacts of two-dimensional and three-dimensional urban morphology on urban thermal environments in high-density cities: A case study of Hong Kong. *Building and Environment*, 252, Article 111249.
- Yan, C., Wan, W.-D., Wang, R.-N., Lai, T.-N., Ali, W., He, S.-s., Liu, S., Li, X., Nasir, Z. A., & Coulon, F. (2024). Quantitative health risk assessment of microbial hazards from water sources for community and self-supply drinking water systems. *Journal of Hazardous Materials*, 465, Article 133324.
- Yang, S., Wang, L., Stathopoulos, T., & Marey, A. M. (2023). Urban microclimate and its impact on built environment – A review. *Building and Environment*, 238, Article 110334.
- Zhang, J., Yu, Z., Zhao, B., Sun, R., & Vejre, H. (2020a). Links between green space and public health: a bibliometric review of global research trends and future prospects from 1901 to 2019. *Environmental Research Letters*, 15, Article 063001.
- Zhang, Y., Yang, X., Yang, H., Zhang, K., Wang, X., Luo, Z., Hang, J., & Zhou, S. (2020b). Numerical investigations of reactive pollutant dispersion and personal exposure in 3D urban-like models. *Building and Environment*, 169, Article 106569.
- Zhang, Y., Gu, Z., & Yu, C. W. (2020c). Impact factors on airflow and pollutant dispersion in urban street canyons and comprehensive simulations: A review. *Current Pollution Reports*, 6, 425–439.
- Zhang, X., Ji, Z., Yue, Y., Liu, H., & Wang, J. (2021). Infection Risk Assessment of COVID-19 through Aerosols Transmission: a Case Study of South China Seafood Market. *Environmental Science & Technology*, 55, 4123–4133.
- Zhang, T., Xu, X., Jiang, H., Qiao, S., Guan, M., Huang, Y., & Gong, R. (2022). Widespread decline in winds promoted the growth of vegetation. *Science of The Total Environment*, 825, Article 153682.
- Zhang, T., Yan, L., Wei, M., Su, R., Qi, J., Sun, S., Song, Y., Li, X., & Zhang, D. (2024). Bioaerosols in the coastal region of Qingdao: Community diversity, impact factors and synergistic effect. *Science of The Total Environment*, 916, Article 170246.
- Zhao, Y., Li, R., Feng, L., Wu, Y., Niu, J., & Gao, N. (2022). Boundary layer wind tunnel tests of outdoor airflow field around urban buildings: A review of methods and status. *Renewable and Sustainable Energy Reviews*, 167, Article 112717.
- Zhao, H., Kong, X., Yao, W., Fei, X., Zhao, J., Zhao, S., & Feng, T. (2023). Control technology of pathogenic biological aerosol: Review and prospect, *Building and Environment*, 243, Article 110679.
- Zhao, R., Liu, J., Jiang, N., & Liu, S. (2024a). Wind tunnel and numerical study of outdoor particle dispersion around a low-rise building model. *Architectural Intelligence*, 3, 1.
- Zhao, Q., Li, R., Cao, K., Yi, M., & Liu, H. (2024b). Influence of building spatial patterns on wind environment and air pollution dispersion inside an industrial park based on CFD simulation. *Environmental Monitoring and Assessment*, 196, 427.
- Zheng, J., Wu, X., Fang, F., Li, J., Wang, Z., Xiao, H., Zhu, J., Pain, C., Linden, P., & Xiang, B. (2021). Numerical study of COVID-19 spatial-temporal spreading in London. *Physics of fluids (Woodbury, N.Y.: 1994)*, 33, Article 046605.
- Zhong, H., Feng, J., Lam, C. K. C., Hang, J., Hua, J., & Gu, Z. (2023). The impact of semi-open street roofs on urban pollutant exposure and pedestrian-level thermal comfort in 2-D street canyons. *Building and Environment*, 239, Article 110387.
- Zhou, D., Song, H., Wang, J., Li, Z., Xu, S., Ji, X., Hou, X., & Xu, J. (2019). Biosafety and biosecurity. *Journal of Biosafety and Biosecurity*, 1, 15–18.
- Zumla, A., Chan, J. F. W., Azhar, E. I., Hui, D. S. C., & Yuen, K.-Y. (2016). Coronaviruses — drug discovery and therapeutic options. *Nature Reviews Drug Discovery*, 15, 327–347.